RAMAN STUDIES OF INTERDIGITATION IN BILAYERS OF CEREBROSIDE SULPHATE

CHRISTOPHER CARL STEVENSON

ISBN 0-315-50471-4

RAMAN STUDIES OF INTERDIGITATION IN BILAYERS OF CEREBROSIDE SULPHATE

by

Christopher Carl Stevenson, B.Sc. (Honours)

A thesis submitted to the School of Graduate
Studies in partial fulfillment of the
requirements for the degree of
Master of Science

Department of Physics
Memorial University of Newfoundland
October 1988

St. John's Newfoundland

ABSTRACT

Spontaneous Raman scattering studies of bilayer systems of the lipid molecule Galactosylceramide I^3-sulphate, or cerebroside sulphate (CBS) in 0.5 and 2.0 M KCl and LiCl solutions in H_2O have been carried out with the samples at temperatures between 10 and 90° C and at thermal equilibrium. By monitoring the intensities of the 2845, 2885, and 2935 cm^{-1} bands in the C-H stretching region of the lipid hydrocarbon chains, packing characteristics of these chains within the lamina of the bilayers are elucidated. For example, the 2885 cm^{-1} band is attributed to the Raman-active asymmetrical stretching mode of CH_2 units along the chains superposed over a broader, intense band due to Fermi resonances with the CH_2 rocking modes at $\approx$1450 cm^{-1}. Drops in the relative intensity of this feature indicate a lessening of the degree of chain-chain interaction in the bilayer, and an abrupt change in this intensity with a change in temperature is an indication that the lipid bilayers have undergone a phase transition with its associated changes in hydrocarbon chain packing. This transition might be between two gel phases, perhaps interdigitated ones, or between a gel phase and the fluid phase.

Unlike for the case of neutrally-charged lipids such as the phosphatidyl cholines, having either symmetric or asymmetric hydrocarbon chain lengths, the observed main phase transition temperatures to the liquid crystalline or fluid state T_m in CBS were only slightly affected by the effective length of the acyl chain attached to the sphingosine base of CBS. This was seen in the differential scanning calorimetry results of J. Boggs *et.al.*, and in the results reported here. T_m depends more heavily on the species of cation in the aqueous environment of the CBS bilayers than on the acyl chain lengths. Potassium, having a smaller

hydrated ionic radius, is found to shield the SO_3^- charge in the CBS headgroup to a larger extent than lithium cations, and this is reflected in a higher gel-liquid crystalline phase transition temperature. Another effect studied is the further increase of T_m through the addition of a single OH group to the carboxyl end of the acyl chain in the saturated 18-carbon species of CBS. The additional inter-headgroup hydrogen bonding is thought to produce this increase in T_m. Finally, the myriad of smaller-enthalpy phase transitions observed by Boggs *et.al* occurring below T_m in their DSC data are not observed here in general; hints of other phase transitions occur only for some CBS samples in K^+, and not for Li^+.

Galactosylceramide I^3-sulphate is a predominant charged lipid in the myelin sheath surrounding axons in the nervous system of all vertebrates. Knowledge of the equilibrium phase behavior of CBS in environments similar to those in nervous tissue would aid those involved in the medical study of nervous disorders, as well as contributing to the understanding of lipid dynamics in general.

ACKNOWLEDGEMENTS

I would like to express thanks to my supervisor, Dr. Nathan H. Rich, for his continued support and financial assistance, to Dr. Joan M. Boggs, The Hospital for Sick Children, Toronto, for her suggestion of this study and for the lipids examined, and to Dr. John P. Whitehead for taking the time to repeatedly discuss the thesis in it's final stages. I would also like to thank Dr. Harry Kiefte and Dr. Maynard J. Clouter, for the use of lab space and facilities; Mike Ryan and Terry White for the manufacture of some of the apparatus; Dr. S. PaddiReddy for lab space when it became necessary to relocate the spectrometer; Dr. Kevin M. W. Keough, for advice and materials; and all of the staff in the Departmental General Office and Mrs. Josephine Barron, for being so patient. Appreciation is also extended to the Physics Department for several Teaching Assistantships and to the Department of Graduate Studies, Memorial University of Newfoundland, for a Graduate Fellowship, both of which made this work possible.

TABLE OF CONTENTS

LIST OF FIGURES

LIST OF ABBREVIATIONS

CBS	cerebroside sulphate
C18:0-CBS	non-hydroxylated cerebroside sulphate containing saturated stearic acid.
C18:0h-CBS	hydroxylated cerebroside sulphate containing saturated stearic acid.
C24:0-CBS	non-hydroxylated cerebroside sulphate containing saturated lignoceric acid.
C26:0-CBS	non-hydroxylated cerebroside sulphate containing saturated hexacosanoic acid.
DMPC	di myristoyl phosphatidyl choline.
DPPC	di palmitoyl phosphatidyl choline.
DSC	differential scanning calorimetry.
ESR	electron spin resonance.
MSPC	1-myristoyl 2-stearoyl phosphatidyl choline.
NMR	nuclear magnetic resonance
PC	phosphatidyl choline.
PE	phosphatidyl ethanolamine.
SPM	sphingomyelin.

CHAPTER 1. INTRODUCTION AND BACKGROUND

The concept of the lipid bilayer is a fairly recent one, and in the last few decades interest in this system has grown dramatically out of obscurity and into the forefront of biomedical research. Such bilayers form the basic structural element of the molecular membranes that partition the matter of living systems into functional elements, such as the various organelles in plant and animal cells, and thereby enabling the establishment of the various diffusion gradients and ionic potentials that drive the mechanism of life. Study of the properties of both natural and model molecular membranes is thus directly pertinent to almost any process connected with cellular function, and is currently being carried out by researchers in such diverse fields as solid state physics, spectroscopy, biochemistry, and medicine.

Natural membranes are complex systems composed of essentially two classes of molecules, namely, lipids and proteins. The nature of the lipid portion of these membranes was suggested by Gorter and Grendel in the 1920's. They performed monolayer experiments with lipid extracted from human erythrocyte membranes by introducing the lipid onto a water surface of known area. Lipids are amphiphilic molecules, and spontaneously form a thin film where the water-soluble ends of the molecules are at the surface and the insoluble ends protrude upwards into the air, like soaps which are simple examples of lipids. From their estimation of the surface area of the red blood cells, the area of their monolayer, and other considerations they concluded that erythrocyte membranes were composed of a double leaflet of lipid molecules [1]. Today we know natural membranes to consist mainly of a bilayer of lipid molecules with embedded protein molecules that serve various functions, the proportions and species of both classes of molecule in a given membrane being dependent on the membrane's function [2,3]. For

figure 1.1

Representative illustration of a natural cell membrane, following Singer and Nicolson's fluid mosaic model. (from Weissman and Claiborne, 1975)

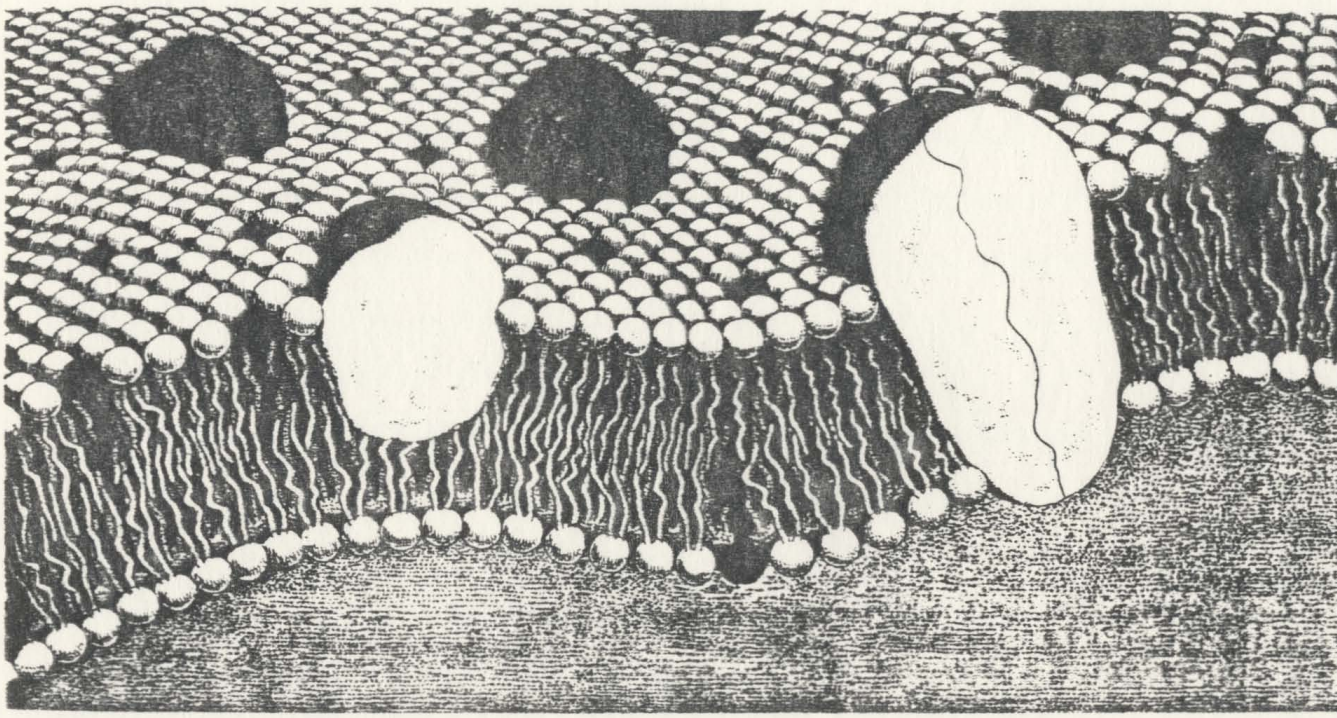

example, the membranes in mitochondria, where metabolic reactions occur in animal cells, have a lipid-to-protein ratio of roughly 1:1 by weight, whereas in the spirally- wrapped myelin membrane surrounding the axons of nerve cells this ratio is closer to 9:1 [4]. This is consistent with the fact that myelin is an insulator, which increases nerve conduction by limiting ion transport across the membrane except at discrete points known as the nodes of Ranvier, so that nervous impulses jump rapidly from node to node instead of propagating at a slower rate down an axon. This insulative property would tend to be disrupted by the presence of proteins in the lipid bilayers. In fact, where ion transport is necessary, certain proteins specifically provide this by forming 'channels' through the membrane [5]. The lipid bilayers are thought to be two-dimensional fluids, as per the fluid- mosaic model of Singer and Nicolson [6] (fig. 1.1). Cholesterol, which is a flat planar lipid molecule shorter in length than most bilayer lipids, exists in varying proportions within the bilayer interior. Its presence seems to have a controlling effect on this fluidity [7] through a range of environmental conditions.

As was mentioned above, lipids are amphiphilic molecules. Typically, each is composed of a polar, and therefore hydrophilic, headgroup and two (or less commonly one) hydrocarbon chains possessing a very low affinity for water and thus described as hydrophobic or lipophilic. Aside from cholesterol there are two main groups of biological lipids, the glycerophospholipids and the sphingolipids. The headgroup of glycerophospholipids contains a phosphate group and is connected to two hydrocarbon chains through a glycerol moiety. The chains, each derived from a fatty acid and either saturated or containing double-bonded carbons, or even having branches [8], are attached at the carboxyl end to carbons 1 and 2 of the glycerol, and the phosphate to carbon 3 (see fig. 1.2a). The two acyl chains are usually of different lengths in lipids found in natural membranes [4, pp 39], and where one of them is unsaturated it is usually the chain closer to the phosphate [9]. The glycerophospholipids predominate in cell plasma membranes, of which those whose headgroups are based on the alcohols choline and ethanolamine seem to be most numerous [2].

figure 1.2

Representative lipid molecules commonly found in biological membranes.

a) A typical glycerophospholipid, di myristoyl phosphatidylcholine.

b) A sphingolipid, in particular one of the lipids in the current study; α-hydroxy stearoyl galactosylceramide I^3-sulphate, or C18:0h-CBS.

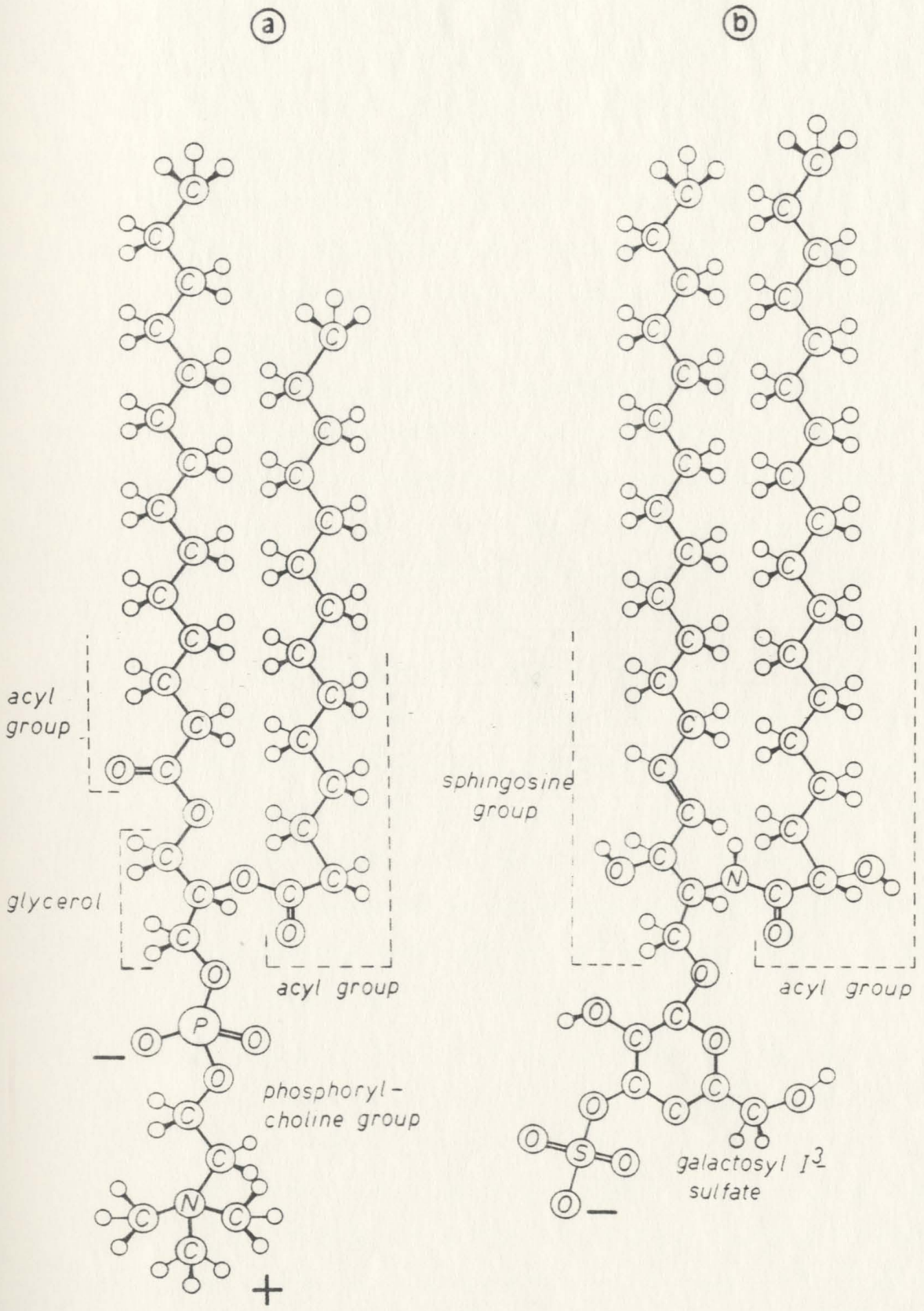
a
b
acyl group
glycerol
acyl group
phosphoryl-choline group
sphingosine group
acyl group
galactosyl I^3_4 sulfate

Sphingolipids are based on ceramide, a derivative of the long-chain alcohol sphingosine with an n-acyl chain attached to the moiety's amide linkage. The sphingosine moiety has a characteristic chain length of 16 carbons, while the fatty acid chain can be of varying length, usually 14 to 26 carbons. The hydrophilic part can be similar to that of the phosphate-containing glycerophospholipids, as in sphingomyelin, or can be based on a sugar residue in which case the lipid is known as a glycosyl ceramide. A variant of this latter molecule, galactosylceramide I^3-sulphate or cerebroside sulphate (CBS), has a sulphate ion attached to the 3' carbon of the single sugar ring and is the particular lipid of interest in the present investigation (fig 1.2b). The presence of a net negative charge on the headgroup of CBS makes the study of model membranes composed of this lipid attractive, especially when these models are made in ionic solutions containing cations of various species whose concentrations closely approximate the natural environment of CBS in nervous tissues, where it is most commonly found.

CBS is a major charged lipid in myelin, comprising some 3.8% of the lipid found there [10]. Cerebrosides are in general associated with nervous tissue and, though the proportions of the other myelin phospholipids are fairly constant, the amount of cerebroside and cerebroside sulphate present tends to increase with an increase in the complexity of the nervous system. For example, the relative amount of cerebroside and cerebroside sulphate increases from 1.7% in goldfish brain to 13.2% in bovine brain, and from 1.9% in fetal human brain to 14.8% in that of an adult human [2].

Though naturally occuring biological membranes are much more than just the lipid bilayer, much information can be gained through the study of simpler model membranes prepared from only a narrow range of lipid species isolated from natural systems or, with synthetic preparations, only a single pure lipid. In making a model system, the desired lipid is simply dispersed in water or a buffered ionic solution based on water. Owing to the amphiphilic nature of lipid molecules, the polar headgroups interact with the surrounding medium through

hydrogen bonding and become hydrated, while the acyl chains do not, and the molecules spontaneously assemble either in micelles or bilayers (fig. 1.3). Micelles are formed chiefly by singly-chained lipid molecules, being tiny ellipsoids of lipid whose average radius roughly equals the lipid molecule's length. Micellar dispersions appear transparent because this diameter is only on the order of 10 nm, and scattering of visible light is not favored. Large-headgroup lipids such as detergents exhibit this packing arrangement; smaller headgroup single-chain lipids can form globular or cylindrical micelles as well. Double-chained lipids generally form lamina in an arrangement where two such lamina are lying next to one another with the hydrocarbon sides adjacent in order that they remain isolated from the aqueous environment and that their conformation remain an energetically favorable one. These bilayers close off to form either singly or more commonly multilamellar spherical envelopes of trapped water. An exception to this are small-headgroup double-chained lipids, such as di-acyl phosphatidyl ethanolamine, which can form inverted cylindrical micelles [11]. By using ultrasonic radiation of a sufficient power, a process called sonication, multilamellar vesicles can be reduced to smaller, singly lamellar ones; the two forms of dispersion have somewhat different dynamics [12].

Primarily due to the various packing geometries and intrachain configurations possible in the hydrophobic center of bilayers in an aqueous environment, model lipid bilayers can be found in any of several different temperature-sensitive morphological phases. In the simplest approximation, for a model bilayer system consisting of two-chained lipids where each chain is identical, the situation can be treated essentially as an Ising problem. This has been done by Pink *et.al.*, Lee, and others [13-15], and Nagle has pointed out certain considerations and criticisms of this approach [16]. The theoretical model has only two lipid phases, the solid and fluid phase, arising from lipid chains in only two states; an unexcited, linear all-*trans* state and an excited, kinked *gauche* state, where *gauche*-rotations about the carbon-carbon bonds in the chain are present and as a result the chains do not pack as efficiently. There is further

figure 1.3

Typical structures formed by lipids in an aqueous environment.

a) Spherical micelles.

b) Cylindrical inverted micelles

c) Bilayers; illustrated is a multi-lamellar bilayer vesicle.

impressed upon the system an overall potential representing the attractive forces at the lipid headgroups, due to the hydrophobic effect, that hold the bilayer together. One sees both in this mathematical model and in observations of real systems a sharp transition between a phase where most of the system is all-*trans* to one where most of the system is fluid, at a critical temperature T_m. More complex behavior is seen as well, however, for these di-acyl PC systems, and from X-ray diffraction data it is seen that in what is termed the $L_{\beta'}$ phase the lipid molecules' long axes are at an angle of about 35^o to the bilayer normal and not parallel to it as the Ising model assumes [16;17,18]. Upon heating, these systems re-order and adopt an intermediate ordered ripple, or $P_{\beta'}$ configuration about $5–10^o$ C prior to the main transition into the two-dimensional fluid L_α liquid crystalline phase (fig. 1.4a; see, for example, [7]). Phosphatidyl ethanolamine bilayers do not exhibit this chain tilt, nor do they show any pre- transition; this is probably due to that lipid's smaller headgroup [19].

Even more complex behavior is possible. Generally the two chains in most lipid molecules are of dissimilar lengths, and the question of chain packing becomes a somewhat more involved one. Even in a symmetrical PC such as dimyristoyl phosphatidyl choline (DMPC), a 90^o bend in the *sn*–2 chain at the glycerol moiety introduces an effective chain length difference of some 0.34 nm, or three CH_2 residues. Such asymmetry introduces the possibility of interdigitated chain packing, where either the long and short chains of lipid molecules in opposing sides of the bilayer meet end-to-end (partial), or the short chains meet with only the long chains being interdigitated across the bilayer center and into the opposite leaflet (mixed). The former packing scheme retains a chain density of two chains per headgroup, and the latter one is a little tighter with three chains per headgroup [20]. It has also been suggested that full interdigitation might occur for both single- and double-chained lipid molecules if their headgroups were either large enough or far enough apart [21]. This would have the effect of creating a large amount of 'empty' space in the hydrophobic region of the bilayer, which could be filled if the chains or pairs of chains packed together side by side.

figure 1.4

Thermotropic phase behaviors of model lipid bilayer systems upon heating.

a) Symmetric chain-length phosphatidylcholine bilayers, with the characteristic chain tilt in the two gel phases.

b) Asymmetric chain-length lipid bilayers, such as for sphingomyelin, showing two types of lipid chain interdigitation.

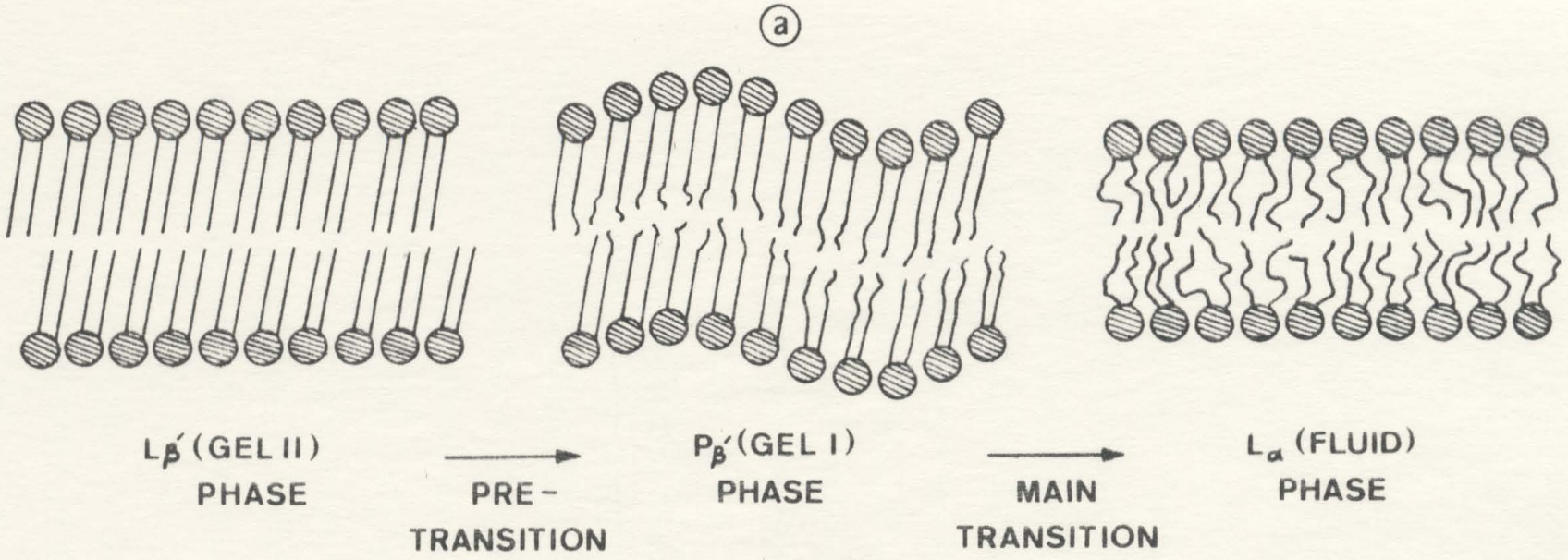
(a)
$L_{\beta'}$ (GEL II) PHASE
PRE-TRANSITION
$P_{\beta'}$ (GEL I) PHASE
MAIN TRANSITION
L_{α} (FLUID) PHASE
(b)
GEL II MIXED INTERDIGITATED
GEL I PARTIALLY INTERDIGITATED
FLUID PHASE

Thus, for two-chain lipid molecules, this gives four hydrocarbon chains per headgroup. Evidence of this complete interdigitation exists in X-ray diffraction studies of bilayers of DPPC in concentrated glycerol and ethylene glycol solutions [22] for example.

Many studies of the phenomenon of interdigitated chain packing have been undertaken. Using Raman spectroscopy to study water dispersions of PC's with asymmetric chain lengths Huang *et.al.* [23] inferred interdigitated chain packing from variations in the degree of asymmetry of the change in vibrational coupling between the hydrocarbon chains during the main phase transition. This coupling, whose magnitude reflects the degree of packing order among the chains, was found to change the least for species of PC in which the sn-2 chain was 4 CH_2 units shorter than the sn-1 chain (see fig. 1.2), and to increase thereafter with increasing asymmetry. They argued that this was indicative of the adoption of a partially interdigitated packing arrangement; in a non-interdigitated arrangement the ends of the longer chains are free to develop dis-ordering *gauche*-conformers. Other work by Hui *et.al.* [20] on these same systems using X-ray diffraction found the bilayer thicknesses of the C18:C(2n) PC bilayers to be roughly comparable to that of C14:C14 PC (DMPC) bilayers in the fluid phase, but considerably less below T_m, for n=5 to 9. They proposed both a mixed and partial interdigitation model, depending on the specific lipid species and bilayer hydration, in general agreement with the Raman results.

The second major class of biological lipids, the sphingolipids, are usually asymmetric and to this end a good deal of attention has been given to them. Lignoceroyl sphingosyl phosphatidylcholine (C24:SPM), a sphingomyelin having a saturated 24-carbon acyl chain in addition to the 16-carbon sphingosine chain, has been examined in hydrated bilayers by Levin *et.al.* [24] using Raman spectroscopy as previously described. Under similar conditions and using similar data analysis procedures as in the above-mentioned PC studies, they observed two distinct transitions at 48.5 and 54.5^o C respectively. C24:SPM is highly asymmetric, so both of the lower temperature phases were interpreted by this group as being

interdigitated ones, the lower temperature phase being a more-highly ordered mixed interdigitated phase and the middle phase being partially interdigitated.

CBS is also a sphingolipid, and highly asymmetric forms of CBS might be expected to behave in a fashion similar to C24:SPM above. The presence of the negative sulphate ion in the headgroup creates a repulsive force between the lipid molecules in the bilayer, however, introducing a difference between SPM and CBS bilayer systems. Possible shielding effects of cations in the aqueous phase of CBS dispersions would lessen this difference. CBS also has the ability to accept one or more additional OH groups, binding them to the interface end of either hydrocarbon chain. The sphingosine base can have one to three hydroxyl groups, and the fatty acid can be α-hydroxylated; the ratio of hydroxy to non-hydroxy fatty acid CBS appears to increase with an increase in nervous system complexity [25], and also with development in human myelin. This ratio in humans ranges from about 1:4 to 8:10 with age. Hydroxylation would further increase the lipid's hydrogen bonding capability, changing the inter-headgroup interaction for example.

Boggs *et.al.* [26-28] have done extensive investigation into the thermal non-equilibrium phase behavior of CBS model membranes in various cation solutions using differential scanning calorimetry (DSC) and electron spin resonance (ESR). They have repeatedly shown using DSC that bilayers of CBS undergo a myriad of large and small endothermic events, interpreted as phase transitions, when slowly heating or cooling the samples and that while these events are complicated functions of such variables as cation type and concentration, acyl chain length, incubation times, and so on, the behaviors is essentially repeatable. From ESR observation of the motion of a long-chain spin probe in the hydrophobic interior of CBS bilayers they have observed behaviors consistent with the interpretation of interdigitated packing schemes. They report that for example the tendency towards mixed interdigitation increases when the fatty acid chain length is increased from 24 to 26 carbons, that hydroxylation of the fatty acid inhibits formation of this phase, and that if a *cis* double bond exists in the fatty acid any form of interdigitation seems to be prevented [28].

In this investigation the determination of the thermal equilibrium phase behaviors of CBS-cation systems similar to those studied by Boggs *et.al.* [26-28] is undertaken for comparison with their DSC and ESR work. One of the incentives for this work was to see if the behavior of the multitude of metastable and stable states observed by this group persisted when studied with Raman spectroscopy and a differing sample history, and thereby arrive at a correlation with their observations of (i) sulphate-ion shielding effects versus cation type and concentration, and (ii) the predominance of headgroup interactions over hydrocarbon chain interactions in establishing the main gel-fluid transition temperature.

Interdigitation from a biophysical standpoint is currently of a great deal of interest because, unlike in the case of symmetric chain lipids, interdigitated bilayer leaflets are more strongly coupled together. There is at this point no conclusive evidence for the biological implications of this, but current speculation includes the possibility of communication of information across biological membranes without the help of proteins, for example.

It was mentioned that interest in biological membrane research is far-ranging, and the techniques employed in experimental work are just as varied. Each technique is best suited for elucidating particular pieces of information. Used frequently in biochemistry, scanning differential calorimetry is a powerful tool for measuring the enthalpy changes that occur in lipid dispersions as a whole when the lipid assemblies change phase. Many subtle re-ordering events can be observed with DSC that are difficult to detect using vibrational methods, the PC pre-transition to the ordered-ripple phase being one such example where on the molecular scale each lipid molecule's environment changes little between the gel-II and gel-I phases. In principle one can also make measurements where the temperature scanning rate approaches zero, that is where the sample is essentially at thermal equilibrium, but in practice this becomes difficult. It is, of course, sensitive to transitions to or from metastable states where they occur, as is evident in Boggs' work on CBS bilayers.

X-ray diffraction, already mentioned several times, is quite usefully employed as a meter stick for measuring, through crystallographic studies, the dimensions of the lipid molecules themselves. It is also used successfully to directly measure the thicknesses of hydrated lipid bilayers; this is invaluable for elucidation of hydrocarbon packing schemes, for example, provided the lengths of the hydrocarbon chains are available. The technique provides a measure against which the inference of such things as interdigitation, as concluded from other methods such as vibrational spectroscopy, NMR, ESR, DSC, and so on, can be checked.

NMR is sensitive to molecular motions occuring on a time scale of 10^{-7} seconds or slower, though theoretically motions ranging from 10^{-12} seconds to several seconds in duration can be studied. Most applicable in NMR is the observation of *trans-gauche* bond rotations in the hydrocarbon chains, and by selective labeling specific parts of the chains can be studied. NMR can also be used to monitor motions of a lipid molecule as a whole, including rotation and 'bobbing' with respect to the molecule's long axis, motions associated with the entire bilayer as a single entity, and the lipid "flip-flop" between leaflets of the bilayer. Care must be taken, however, that the sampling time be chosen judiciously otherwise anisotropic motions can average out to look like isotropic ones.

Biological molecules are not intrinsically paramagnetic and thus do not lend themselves to ESR studies unless a spin label is used, in which case motions of the label induced by the bilayer on time scales of $10^{-8} - 10^{-11}$ seconds can be studied. Thus, ESR results pertain more to a fluid hydrocarbon environment within the bilayer. While the information thus gained is valuable, by introducing a substance into the system the resultant perturbations can have an effect on the obtained results. The same is true for fluorescence studies, except that the fluorophores employed there are even larger than most ESR spin labels. Fluorescent techniques are valuable for determining such things as lateral motion within a bilayer, a process measured on a time scale of minutes, or specific study of the bilayer molecular conformations by measuring the fluorophore's decay half-life, usually on the order of 1-100 ns.

Infrared absorption spectroscopy is a powerful technique for looking in detail at normal vibrations of various parts of a molecule. However, up until recently infrared studies of biological systems have been severly limited by the fact that most of these systems are found in aqueous environments and the attendant strong water absorption bands make collecting lipid spectra very difficult. In an effort to make gains in this field for biological research much effort has gone into the preparation of samples in thin layers and increasing the signal to noise ratio by using Fourier spectroscopic techniques. Raman spectroscopy is also a powerful technique as it too monitors specific molecular vibrations, motions on a time scale of 10^{-15} seconds, but has the advantage that it employs visible light in the scattering process. As water does not appreciably scatter visible light Raman spectra are relatively free of the effects of the water in lipid dispersions. Raman spectroscopy would seem to be an ideal tool for biological membrane research, partly because in practice it is relatively simple both to implement and to interpret results. It does have its own experimental difficulties, especially due to the opacity of lipid dispersions and the large amounts of elastically scattered light and fluorescence that result. Raman and infrared spectroscopy are clearly complementary methods of investigation and both are important.

Specifically, the approach taken in this investigation is that of vibrational spectroscopy. Raman scattering methods are employed to monitor changes in the C-H stretching normal vibrations of the many CH_2 and terminating CH_3 units in the hydrocarbon chains of CBS assembled in lipid bilayer in ionic solutions of the cations potassium or lithium. Each observation is done at constant temperature and compared with the DSC results due to Boggs, *et. al.*, already mentioned. Relative order in the hydrocarbon region of the model membranes is quantified by defining two order parameters, the ratios of the intensities of vibrational modes sensitive to the degree of interchain interaction, and these quantities are then compared to those obtained by other researchers for asymmetric phosphatidyl choline and sphingomyelin bilayer systems, as well as for the simple symmetric PC system DPPC. From the Raman data the intra-chain conformation-

dependent shift in the frequency of one C-H stretching mode, that of the asymmetric CH_3 mode, is also monitored. Interdigitation as indicated by these results for species of CBS containing non-hydroxylated fatty acids with chain lengths of 18, 24, and 26 carbons is discussed, both with reference to the cation used in the dispersion buffer and its concentration, and the chain length. The effect of α-hydroxylation in the 18 carbon variety of CBS is also investigated.

Present in the data as well was an unusually intense background feature underlying all of the C-H stretching modes of the lipid chains. A separate investigation was launched in an attempt to identify the cause of this feature. The broad background peak, which was mathematically removed from the digitally-collected data before the order parameters were calculated, is thought to be due to O-H stretching at the headgroup-water interface perhaps by the abundance of hydrogen bonding sites in CBS.

In the following chapters of this dissertation are discussed some theoretical considerations regarding Raman scattering and lipid systems in Chapter 2, and the details of the experimental apparatus and procedures used in Chapter 3. In Chapter 4 the results of the spectroscopic observations are presented and discussed, and the work is then summarized.

CHAPTER 2. THEORY

2.1 Spontaneous Raman Scattering

Electromagnetic radiation and matter can interact in a number of ways. There are essentially three processes whereby this occurs; photons can be absorbed by an atom or molecule, exciting it, and they can subsequently be emitted again either (i) spontaneously, (ii) through stimulated emission, or (iii) they can be scattered either elastically or inelastically, individually by atoms or molecules and collectively by phonons. It is this third process which is of interest here, and in particular the inelastic molecular process known as Raman scattering.

A semi-classical explanation of light scattering might be as follows. Consider an electromagnetic wave incident upon an atom or molecule. For radiation in the visible range, molecular dimensions are of the order of 10^2–10^3 times smaller than the radiation's wavelength, and so at any given instant in time the atom or molecule finds itself in essentially a uniform electromagnetic field. The electric part of this field displaces the electronic and nuclear charge distributions of the atom or molecule, inducing a dipole;

$$\mathbf{M}=\alpha\mathbf{E}$$

or

$$M_x = \alpha_{xx} E_x + \alpha_{xy} E_y + \alpha_{xz} E_z$$

$$M_y = \alpha_{yx} E_x + \alpha_{yy} E_y + \alpha_{yz} E_z$$

$$M_z = \alpha_{zx} E_x + \alpha_{zy} E_y + \alpha_{zz} E_z$$

where α is the molecule's polarizability. $\mathbf{E}$ is periodic in time, and the resulting

oscillating dipole emits radiation of the same frequency as the incident radiation if for the moment we regard α as being a constant. This type of scattering is elastic Rayleigh scattering, which while useful for some purposes doesn't concern us here as it yields little information about intramolecular dynamics.

Molecules undergo many types of motion, including translational, rotational, and vibrational motion. Vibration in particular involves periodic changes in the internuclear spacings within a molecule, which in turn will change the polarizability tensor α. To a first order approximation then, we might have for the case of a simple diatomic molecule

$$\alpha_{zz}(t) = \alpha_{zz}{}^{o} + \frac{d\alpha_{zz}}{dr}\Delta r(t)$$

$$= \alpha_{zz}{}^{o} + \frac{d\alpha_{zz}}{dr}\Delta r_{\max} cos(2\pi c\, \nu_{vib}\, t)$$

where α^{o} is the equilibrium polarizability of the molecule, ν_{vib} is the vibrational frequency, and $\Delta r_{\max}$ is the maximum change in the equilibrium nuclear separation of the two nuclei. Following this through, if we assume that only α_{zz} is non-zero, and if the incident light is polarized in the x-y plane and propagates along the z-axis with frequency ν_i,

$$E_z(t) = E_{\max} cos(2\pi c\, \nu_i\, t)$$

we have

$$M_z(t) = \alpha_{zz}{}^{o} E_{\max} cos(2\pi c\, \nu_i\, t)$$

$$+ \frac{d\alpha_{zz}}{dr}\Delta r_{\max} cos(2\pi c\, \nu_i\, t) cos(2\pi c\, \nu_{vib}\, t) E_{\max}$$

which, using the cosine identity

$$\cos A \cos B = \tfrac{1}{2}(\cos(A+B) + \cos(A-B))$$

becomes

$$M_z(t) = \alpha_{zz}{}^{o} E_{\max} cos(2\pi c\, \nu_i\, t)$$

$$+ \tfrac{1}{2}\frac{d\alpha_{zz}}{dr}\Delta r_{\max} E_{\max} cos(2\pi c t\, [\nu_i + \nu_{vib}])$$

$$+\tfrac{1}{2}\frac{d\alpha_{zz}}{dr}\Delta r_{max}E_{max}cos\,(2\pi ct\,[\nu_i-\nu_{vib}\,])$$

The first of these terms is the Rayleigh term; the following terms are the anti-Stokes and Stokes Raman terms, respectively. This simple approach fails, however, to explain the observed difference in intensity between scattered light arising from these latter two terms, as the Stokes radiation is more pronounced than the anti-Stokes. To partially resolve this, we turn to a quantum picture of what is happening.

In a Stokes scattering transition, an incident photon can be thought of as causing a transition from some state, be it vibrational or rotational, of an atom or molecule, to some higher virtual excited state, followed immediately by a transition back down to the excited state above the initial one. The decrease in energy of the photon is equal to the energy difference separating the initial and final quantum states, and is reflected by the decrease of the photon's frequency by an amount ν_{vib}. An anti-Stokes transition proceeds in reverse, the scattered photon gaining energy in bringing the molecule or atom from the higher state to the lower one.

Consider vibrational Raman scattering, for example. At temperatures below 10^3K or so, the majority of molecules will be found in their ground vibrational states. The relative population of the first excited vibrational state is given by the Boltzman relation

$$N_1=N_o\,e^{-hc\,\nu_{vib}/kT}$$

where k is Boltzman's constant and T is the absolute temperature; this is a small fraction of the ground state population N_o, and it follows that the number of Stokes transitions is much larger than that of anti-Stokes transitions per unit time. In fact, because N_1 is a function of vibrational frequency, one has difficulty in even detecting anti-Stokes lines past around $1000cm^{-1}$ due to their low intensities [29,30].

The expression for the polarization tensor can more formally be written in terms of the normal vibrational coordinates Q_k of the molecule;

$$\alpha = \alpha_o + \sum_k \left(\frac{\partial \alpha}{\partial Q_k} \right)_o Q_k$$

to first order. In light of our original equation, and assuming that a vibrational molecular wavefunction ψ^n is a product of the respective wave functions for the normal modes, represented by the Hermite polynomials;

$$\psi^n = \prod_k \psi_k{}^n$$

we can then write

$$\int \psi^n \mathbf{M} \psi^m \, d\tau = \mathbf{E} \int \psi^n \alpha \psi^m \, d\tau$$

$$= \mathbf{E} \alpha_o \int \psi^n \psi^m \, d\tau + \mathbf{E} \sum_k \left[\left(\frac{\partial \alpha}{\partial Q_k} \right)_o \int \psi^n \, Q_k \, \psi^m \, d\tau \right]$$

Because the molecular wavefunctions are orthogonal, the first of these integrals is zero unless ψ^n and ψ^m are identical; this corresponds to no change of state, and is the Rayleigh term. The $\left(\frac{\partial \alpha}{\partial Q_k} \right)_o$ are constants; it is the Q_k that change over time (due to molecular vibrations). If we expand the last integral, it becomes apparent that all of the individual $\psi_k{}^n$'s and $\psi_k{}^m$'s must be identical except for the k^{th}, where because the ψ_k's are assumed to be Hermite polynomials they must differ only by $\Delta v = \pm 1$ in order that this integral be non-zero.

This simple selection rule is not adhered to strictly by real molecules, however, because real vibrations are not confined to the harmonic approximation within which the Hermite polynomials are assigned as wavefunctions. Also, the Taylor expansion for α might involve higher terms than just the linear one. For example, if this expansion involved $\left(\frac{\partial^2 \alpha}{\partial Q_k{}^2} \right)_o$, then

$$\int \psi_k{}^n \, Q_k{}^2 \psi_k{}^m \, d\tau = 0$$

except where $\Delta v = \pm 2$ for Hermite polynomials [31]).

2.2 Hydrocarbon chain vibrational spectra

Lipid molecules are large entities, and consequently have many normal modes of vibration arising from the various parts of the molecule, such as the headgroup or hydrocarbon regions. As such, a rigorous analysis of biological molecules, such as lipids, as a whole is prohibitively complex and we seek to understand the dynamics of these molecules by first analyzing simpler systems that approximate some portion of the large molecules and applying by analogy what is learned.

As seen in fig 2.1, the vibrational Raman spectrum of a typical lipid dispersed in water is a collection of modes arising from all parts of the molecule, but is dominated by those modes associated with the normal vibrations of the lipid hydrocarbon chains. It follows that a detailed understanding of isolated hydrocarbon chains is desired.

A long chain molecule can be thought of as a linear arrangement of a large number M of repeat units. If each unit cell contains n atoms, then there are 3nM possible vibrational modes divided into 3n frequency branches. Within each branch are M vibrational modes whose precise frequencies depend upon the relative phase of the nuclear displacements of one unit cell to the next, given by

$$\phi_k = k\pi/M, \qquad k = 0,1,2 \ldots M-1$$

For the polyethylene zig-zag chain, the unit cell is ethylene, C_2H_4, and so as n=6 there are 18 frequency branches for arbitrary ϕ_k. Alternatively, we could say that the unit cell is CH_2 with ϕ_k = multiples of π, giving 9 branches where $\phi_k = 0$ or π.

For infinite polymers it can be shown that only those vibrations for which the nuclear displacements along the chain axis of each unit cell are identical, that is for which $\phi_k = 0$, are allowed in the Raman or infrared spectrum. The vibrations corresponding to this have k=0, and in non-infinite polymers these

figure 2.1

Raman spectrum of a typical lipid, and of a theoretical analogue, paraffin. 514.5 nm excitation at ≈70mW.

a) DPPC, at 30° C. Recorded at 0.5 cm^{-1}/s, 2 s count integration time.

b) Paraffin, at 30° C. Recorded at 1.0 cm^{-1}/s, 1 s count integration time.

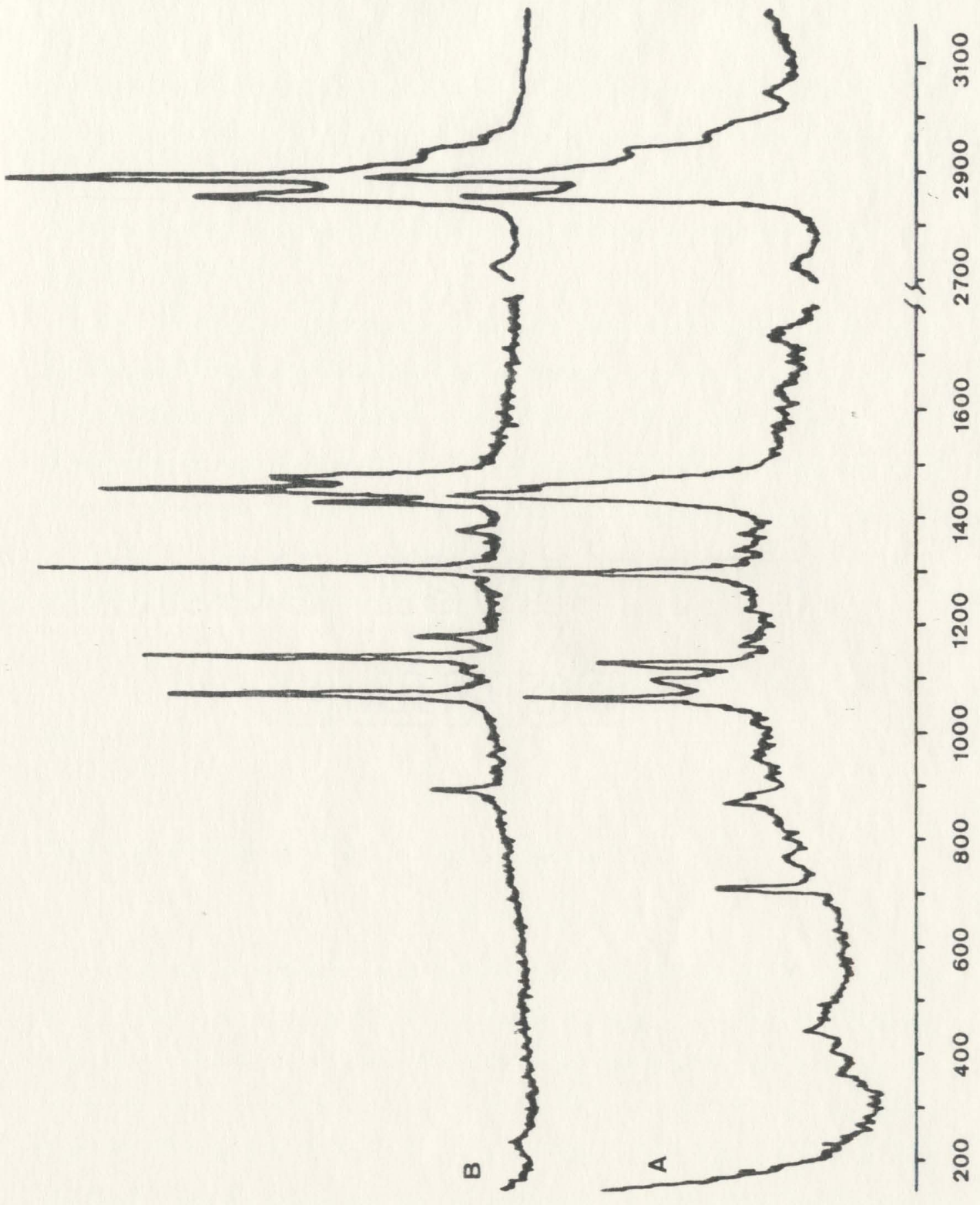
B
A
200
400
600
800
1000
1200
1400
1600
2700
2900
3100

vibrations are the most intense. The observed intensity decreases as ϕ_k departs from zero, and k=1 and 2 vibrations are also weakly observed [32]. If, through the generation of *gauche*-conformers the average effective M of all-*trans* segments in the chain is greatly reduced, ϕ_k can take on a variety of values; the average ϕ_k value shifts up from zero, and the frequency of a given vibrational mode changes accordingly. This fact is used by some researchers to monitor the effective all-*trans* lengths of lipid chains as a function of temperature and other variables [eg.,33-35]

The various normal modes of vibration have been calculated by many researchers for both the ideal case of infinite-length polyethylene chains and the more realistic case of finite-length paraffins [36-39]. An example of one approach is presented in work by Snyder and Schachtshneider [36,37]. They proceed using Wilson's G-matrix method, which starts with the vibrational problem description in internal coordinates R and continues by describing the kinetic and potential energies of the system in terms of these;

$$2T = \frac{d}{dt} R' G^{-1} \frac{d}{dt} R$$

and

$$2V = R'FR.$$

They then write the vibrational secular equation as

$$GFL = L\Lambda$$

where L is the transformation matrix from the normal coordinates Q to the internal coordinates R (R=LQ) and Λ is a diagonal matrix of the various frequency parameters involved. They then solve this secular equation. A calculated phonon dispersion curve due to Lippert and Peticolas [32] for infinite polyethylene zig-zag is presented in fig. 2.2; for finite chains several more vibrational modes occur than are shown here due to the presence of terminating methyl groups, as is seen in real spectra and Snyder's calculations.

figure 2.2

Calculated phonon dispersion curve for infinite chain-length hydrocarbon zig-zag, polyethylene (from Lippert and Peticolas).

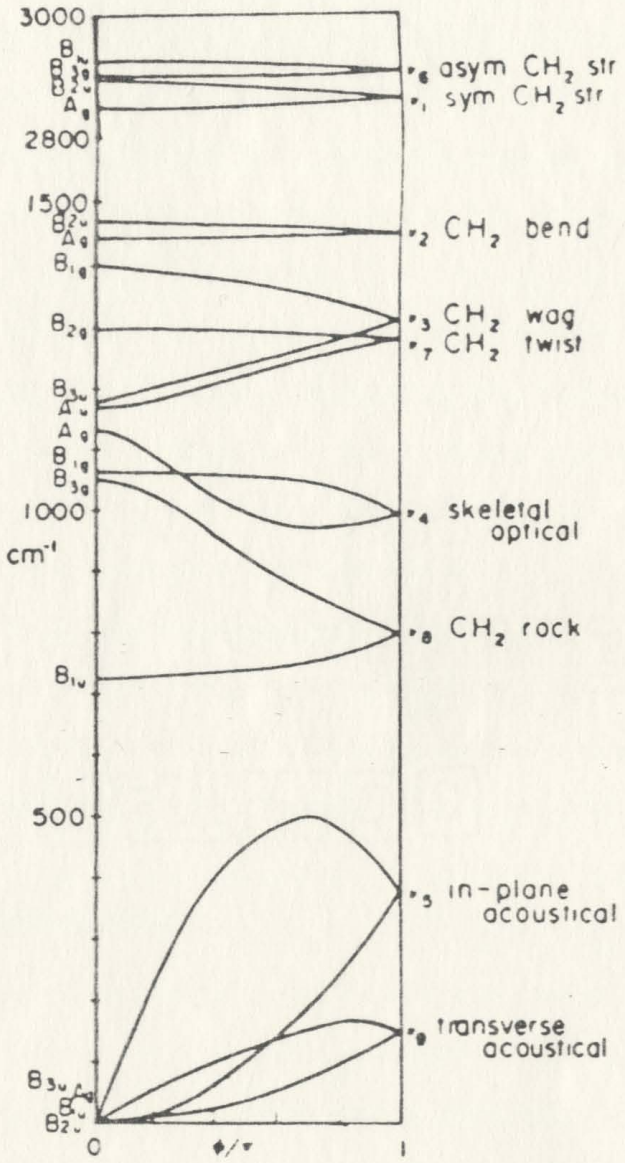
3000
2800
1500
1000
cm⁻¹
500
0
1
ν6 asym CH2 str
ν1 sym CH2 str
ν2 CH2 bend
ν3 CH2 wag
ν7 CH2 twist
ν4 skeletal optical
ν8 CH2 rock
ν5 in-plane acoustical
ν9 transverse acoustical

The hydrocarbon chains of lipid molecules in the ground state can be treated as good approximations of infinite polyethylene zig-zag, and so we assign the vibrational modes of polyethylene, or more properly the long-chain paraffins, to them by analogy. Some care should be exercised here, however, because lipid chains are motionally constrained at one end where they join the remainder of the molecule. Of more profound consequences is the fact that some of these normal modes are affected by interchain vibrational coupling as a result of the close chain packing found in lipid bilayers or some micelles. Where one mode has a frequency half that of another, for example, this coupling can result in Fermi resonances between modes. As one might expect, the development of *gauche* rotations in the chains would have a decoupling effect; this, and the already-mentioned point that the frequencies of the coupled vibrations themselves begin to shift upon formation of *gauche*-conformers and might no longer resonate, would cause a marked decrease in the magnitude of CH_2-related Fermi resonance features present in the ground-state lipid bilayer spectra. By monitoring the intensity of vibrational modes dependent on interchain interaction, then, one can measure both the relative configurational disorder in the chain packing, and the conformational disorder in the hydrocarbon chains themselves.

2.3 Skeletal Optical Modes

A particular region of interest for studies of intra-chain disorder, the skeletal optical modes, are found between 1050 and 1140 cm^{-1}. For straight, all-*trans* chains the three predominant features seen in this region are the out of phase $(\phi_k = \pi) B_{2g}$ transverse C-C stretching mode at 1062 cm^{-1}, the in phase $(\phi_k = 0) A_g$ transverse stretching mode at 1130 cm^{-1}, and a weaker all-*trans* mode at 1100 cm^{-1}. When *gauche* rotations about C-C bonds are excited either thermally or by perturbations from other substances in the bilayer, a new feature appears at $\approx$1090 cm^{-1} and the intensities of the all-*trans* bands fall off. The wavenumbers of the 1130 and 1100 cm^{-1} features also shift downwards, both being a function of the effective chain length [12]. Thus, this spectral region is

well suited to studies of intra-chain conformational changes but changes in the chain packing itself can only be inferred.

2.4 C-H Stretching Region

Of interest here is the high-frequency region from 2800 to 3100 cm^{-1}, associated with the various C-H stretching modes [12]. Most easily discerned are two sharp and intense CH_2 stretching features, the symmetric and asymmetric modes at 2845 and 2885 cm^{-1} respectively, and one symmetric and two asymmetric CH_3 stretches at 2935, 2945, and 2967 cm^{-1} respectively. Because of vibrational coupling effects between the packed chains, however, other more broad features arise. One, an intense mode centered at 2885 cm^{-1}, is due to a Fermi resonance between the symmetric CH_2 stretch and an appropriate combination of methylene bending fundamentals at $\approx$1450 cm^{-1}. Upon the appearance of chain-decoupling *gauche* conformers this feature virtually disappears, and the intensity of the composite 2885 cm^{-1}-band lessens greatly. With the appearance of the C-C bond rotations an IR-active CH_2 symmetric stretching mode at 2938 cm^{-1} becomes Raman-active due to symmetry loss in the chains. In addition, there is also a feature at this frequency due to a Fermi resonance between the terminal methyl symmetric C-H stretch and the CH_2 deformation modes at $\approx$1450 cm^{-1}. The vibrational coupling responsible for this resonance tends to increase with *gauche* conformer formation, and so the composite 2935 cm^{-1} feature *increases* in intensity upon the chains melting into a fluid state at T_m. There is as well a 10 to 12 cm^{-1} shift upwards in the wavenumber of the asymmetric CH_3 stretching mode to $\approx$2896 cm^{-1}. However, the 2845 cm^{-1} methylene symmetric stretching feature remains essentially unchanged through the transition of the packed chains to the fluid state, and for this reason is used as a reference. It should be noted here that monitoring the skeletal optical region for the chain ordering changes that accompany various bilayer phase transitions provides the same information on *gauche*-bond formation as the C-H stretching region. The choice of the latter over the former region was dictated partly by the presence of

vibrational coupling effects in the C-H region which seem appropriate to a study of chain packing characteristics.

As is a standard practice in lipid Raman spectroscopy (eg., Levin [12]), the chain packing characteristics of lipid bilayers are monitored in this investigation by comparing the intensities of the 2880 and $2935 cm^{-1}$ feature intensities with each other to form a sensitive indicator of the degree of interchain order and disorder, respectively. Also employed is the intensity of the former feature in comparison to the relatively constant intensity of the $2845 cm^{-1}$ symmetric CH_2 C-H stretch feature. The two order parameters thus defined are

$$R_1 = \frac{I_{2935}}{I_{2880}} \quad \text{and} \quad R_2 = \frac{I_{2845}}{I_{2880}}$$

In practice these Raman intensities are measured as amplitudes; the height of a spectral feature above its local background is measured as opposed to the area underneath it, though in the skeletal optical mode region where the separate features are distinguishable some researchers employ area measurements [34]. There is no direct physical content in these order parameters, it should be stressed, and their use comes in comparing their values obtained for an unknown system with those for a system well-characterized by many investigative methods.

Because the lipids are dispersed in H_2O, one might expect a Raman signal from this latter molecule as well. For free water an O-H stretching feature is seen very close to the hydrocarbon C-H stretching modes, at $\approx 3370 cm^{-1}$. This Raman feature is thought to actually be a superposition of two different O-H stretching features, due to different hydrogen-bonded water structures [40,41]. In the Raman spectra of water dispersions of phospholipids such as DPPC this broad composite feature is weakly observed and poses no problem as far as interference with the C-H stretching region is concerned. However, when Raman spectra were collected in this study for water dispersions of CBS an intense feature very much like the free-water O-H stretch at $\approx 3400\ cm^{-1}$ is observed, only shifted downwards in frequency to $3000\ cm^{-1}$, and where there is an extra OH group present

at the CBS molecule interfacial region, further shifted another 100 cm^{-1} to 2900 cm^{-1}, making analysis of the C-H stretching region much more difficult and necessitating the mathematical fitting and subsequent subtraction of the feature from the spectra. The feature, how it is dealt with, and where it might arise from are discussed in further sections.

CHAPTER 3. APPARATUS AND EXPERIMENTAL TECHNIQUE

Raman Scattering

Lipid vibrational spectra were collected using the Raman spectrometer represented schematically in fig. (3.1). Because of the opaque nature of the lipid dispersions, a backscattering arrangement was adopted where a short focal length ratio cassegrain system collected scattered radiation over a large solid angle at 180 degrees to the direction of the incident exciting radiation. In brief, the spectrometer consisted of an argon ion laser as a monochromatic light source, a temperature-controlled sample holder placed at the focus of the laser beam, wide-aperture collection optics, a double monochromator to disperse the scattered light, and a thermoelectrically-cooled photomultiplier tube operated with a pulse shaper/discriminator in photon counting mode. The spectra were digitally recorded to a tape drive, and later downloaded to a VAX 8800 for subsequent analysis. This arrangement is described in more detail in the following sections.

3.1 Source

Two slightly different sources were used in the course of this research, though because the resolution requirements of the lipid Raman spectra were not very stringent, they could be used interchangeably. Both were water-cooled argon ion lasers (Spectra Physics model 165, and Continental Laser Corporation 3000 series), operated with a prism in the laser cavity to select the green 514.5 nm line. The Spectra Physics laser was simultaneously used for a separate unrelated research project requiring narrow linewidths, and so included in the cavity a temperature-regulated etalon assembly (Spectra Physics model 589) for operation

figure 3.1

Schematic diagram of the Raman spectrometer and associated apparatus used in this investigation.

S_1	Thermoelectric cooler power supply (7.0 A).
S_2	Photomultiplier tube high voltage supply (1750 VDC).
F	10.0 nm - bandpass 514.5 nm filter.
C	Cassegrain collection optics.
PMT	Ga-As photocathode RCA 31034 photomultiplier tube.
SB	Data switch box.
SC	Sample cell.

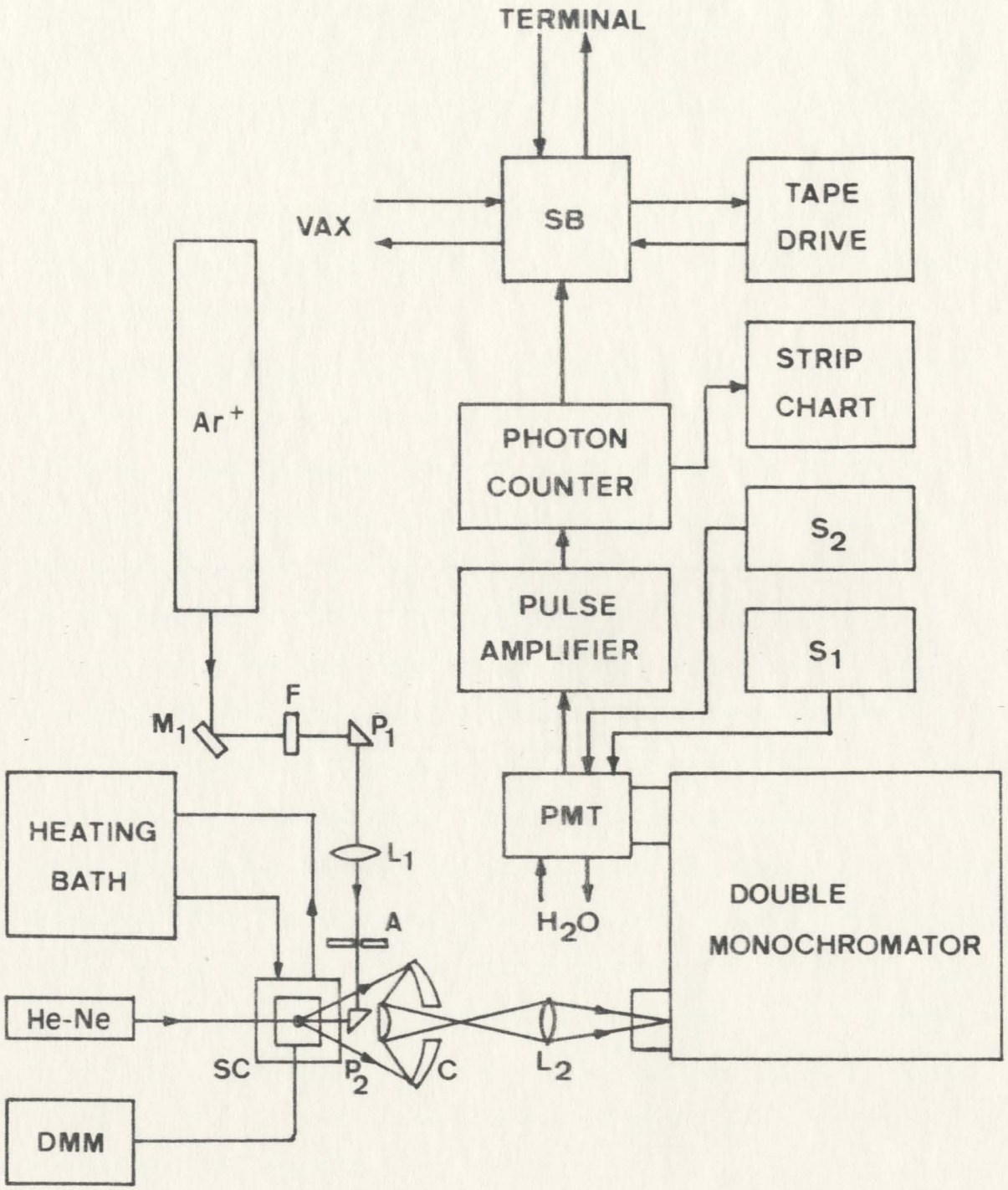
TERMINAL
SB
VAX
TAPE DRIVE
STRIP CHART
PHOTON COUNTER
Ar+
S2
PULSE AMPLIFIER
S1
F
M1
P1
HEATING BATH
PMT
L1
DOUBLE MONOCHROMATOR
A
H2O
He-Ne
SC
P2
C
L2
DMM

in single mode, whereas the latter laser was operated in multi-mode. Tube currents and output powers were on the order of 30 A and 300 mW for the former, from which 200 mW was used via a flat beam splitter, and 16 A and 150 mW for the latter which was used directly. Both lasers had outputs that were polarized in the vertical direction; this matched the direction of the rulings of the gratings used in the double monochromator, and so allowed for maximum throughput to the photomultiplier. No attempt was made to scramble the polarization of the light scattered from the sample before it entered the dispersive portion of the spectrometer.

Because of the very high levels of elastically scattered light sent to the monochromator due to both the nature of the sample and the scattering geometry, it was necesary to include a narrow-bandpass filter F in the laser beam before it was focused into the sample cell. Without the filter, argon plasma lines in the laser cavity, with which the spectrometer's collection axis is aligned in the backscattering arrangement through reflection from the sample surface and the glass sample envelope, appear in the spectra obtained. The filter had the undesirable effect of attenuating the incident laser power by some 50-60%, however, so laser power at the sample was of the order of 60-100 mW.

Once directed through filter F by a front-surface aluminum mirror M1, the beam was redirected via prism P1 to a 200 mm focal length lens L1 which focused the 2 mm diameter beam down to a spot on the surface of the sample which averaged 50 μm in diameter. 165 mm from the center of lens L1, directly in front of the collection optics, a small 3 mm right prism P2 sent the beam down the scattering axis 45 mm to the sample tube. An aperture A1 between the lens and this prism blocked extraneous reflections from the prisms, lens, and filter from entering the sample holder.

3.2 Sample Holder and Temperature regulation.

A small sample holder was constructed to keep the lipid samples at a constant, pre-set temperature while holding them in position in the focused laser beam. Essentially, it consisted of a solid block of brass measuring 38 x 38 x 51 mm mounted at the center of a Plexiglas box and insulated with Pyrex wool (see fig. 3.2). The block has a 1.6 mm diameter bore through it horizontally for admission of the incident laser beam, and is widely tapered on the front to allow a large solid angle of scattered light to get to the collection optics. This bore has perpendicular to it, through the center of the block, a 5.6 mm diameter space where the sample tube can be inserted; this passage extends to 2 mm below the beam axis. Parallel to the sample port are six 3 mm diameter holes that run through the block. On the top and bottom of the block these channels are connected together externally with 5 mm O.D. copper tubing into a single 9 mm O.D. copper arm, which leads backwards outside the Plexiglas housing for connection to a temperature-controlled circulating bath. The high flow rate obtained through these heat exchanger channels collectively ensured that the heat transfer through the walls of the 12 mm O.D. Tygon tubing connecting the block to the circulating bath was not a problem. A cladding of polyurethane foam insulation around the tubing was also used to reduce this effect. Four nylon screws were used in mounting the block within the Plexiglas housing. The mass of the block itself provided a large degree of thermal inertia, aiding in the temperature stability of the sample holder. The space between the block and the Plexiglas was filled with Pyrex wool, and the housing was mounted atop a solid 76 mm diameter brass cylinder of sufficient height to bring the scattering port up to the height of the beam; the cylinder was cemented to an aluminum plate with leveling screws.

The circulating bath employed was a refrigerated-type, Lauda K-2/R filled with a 50-50 mixture of tap water and ethylene glycol. This bath provided temperatures down to -11^{o} C and up to 100^{o} C, with temperature stabilities of around ± 0.01 to $\pm 0.02^{o}$ C. Later in the research this was exchanged for a Neslab Endocal RTE-4 refrigerated circulating bath, with similar operating

figure 3.2

Sample cell constructed for holding lipid dispersion sample tubes or capillaries at controlled temperatures for Raman backscattering (to scale).

I Pyrex wool insulation.

N 6/32" Nylon machine screws.

P 1/4" Plexiglas housing.

S lipid sample, in 1.1 mm O.D. Kimax capillary tube.

T Thermistor.

W Pyrex window.

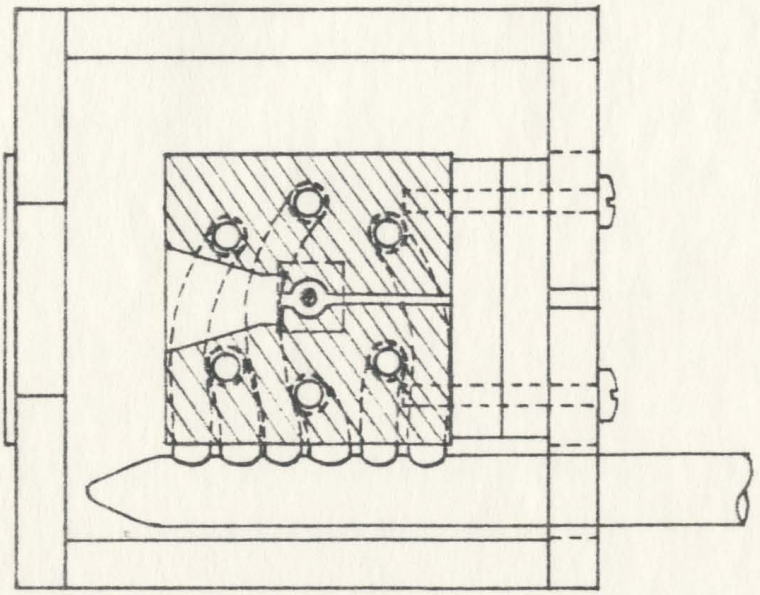

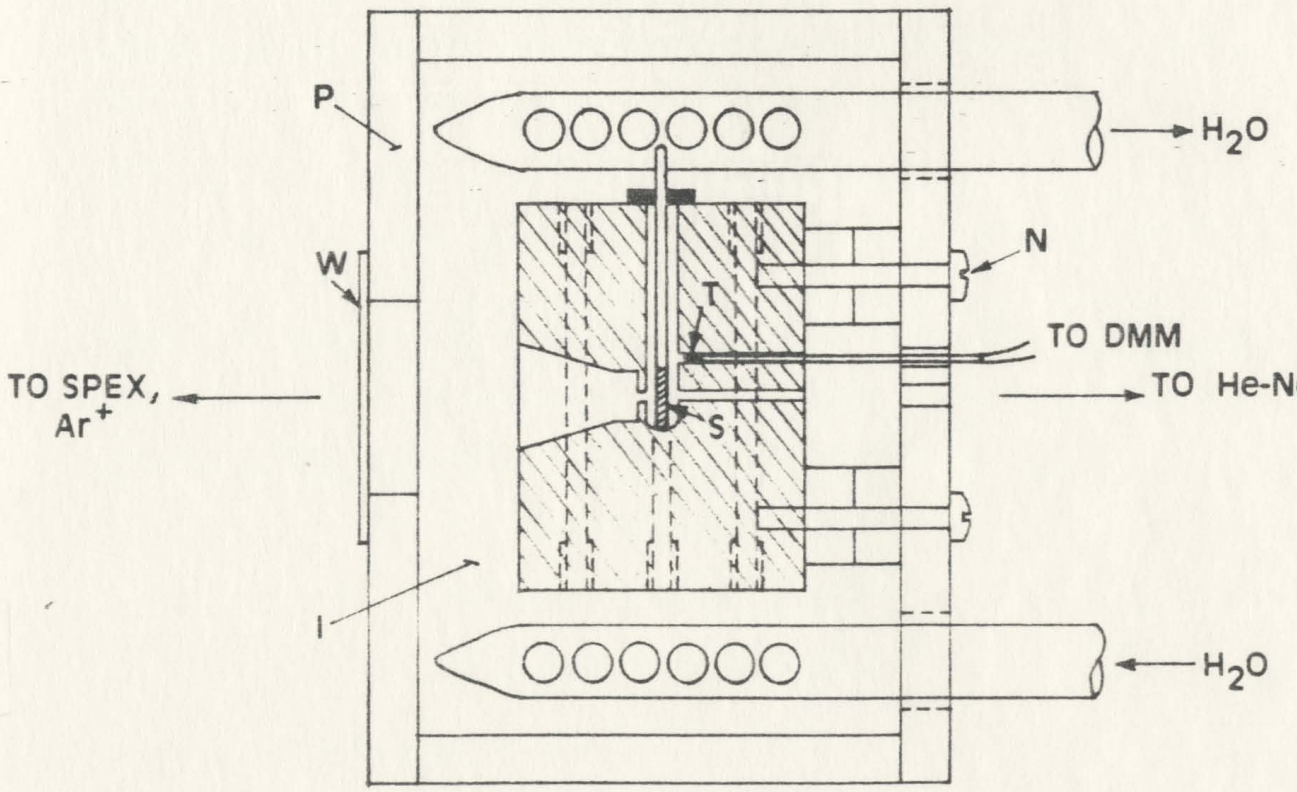
P
W
I
T
S
N
H_2O
H_2O
TO DMM
TO SPEX,
Ar^+
TO He-Ne

characteristics.

Both baths employed proportional-type temperature control, with thermal feedback coming from their self-contained reservoirs.

Parallel to and just above the laser beam port is a 1.6 mm diameter passage leading into the sample chamber. This is for placement of a thermistor as close to the scattering cross-section as possible, though care was taken to ensure that the thermistor (Fenwall) was not being illuminated directly by the high level of elastically scattered light as it was determined that high intensity light affected its resistance somewhat. The thermistor itself was calibrated by heating it in 1^{o} C increments from 12.5^{o} C to 76.5^{o} C, recording its resistance to three or four significant figures with a Keithley 160 Digital Multimeter while simultaneously recording the thermistor temperature with a mercury laboratory thermometer calibrated in 0.1^{o} C divisions. The thermistor was kept in close proximity to the thermometer bulb by physically tying the two together; the coupled pair were immersed in the reservoir of a circulating bath to establish their temperature. The calibration data thus obtained were regressed against the thermistor equation

$$\frac{1}{T} = A + B\ln(R) + C(\ln(R))^3$$

where T is measured in Kelvins, and R is measured in kΩ's. This procedure was done twice to check the calibration, and the constants obtained each time were the same within their standard deviations. These turned out to be

$$A = 0.00317698 \pm 0.00000017\ K^{-1}$$

$$B = 0.00028230 \pm 0.00000065\ K^{-1}$$

$$C = 0.00000127 \pm 0.00000075\ K^{-1}$$

as determined by Minitab release 6.1.1.

3.3 Collection Optics

The optical system employed to collect the light scattered from the sample was a cassegrain telescope assembly (Applied Photophysics Ltd. model 6500), specifically designed and optimized for small source-distance, high aperture work. Essentially, the unit consists of an f/0.42 front surface spherical concave mirror to intercept the scattered light, and a smaller matching front surface convex mirror in front of it to send this light through a 25 mm diameter hole in the primary mirror to a coupling lens at the rear, which is used to match the cassegrain to the f/8 aperture of the monochromator.

Because the sample holder had an aperture of f/1.5, the cassegrain could not be operated at quite its intended optimum source to retro mirror distance of 50-60 mm; it was found that with this distance at 80 mm the light throughput to the photomultiplier tube could be maximized. This corresponds, with the unit's central obstruction, to an effective collection aperture of about f/2. In this configuration the effective magnification of the source was 7-8X.

3.4 Double Monochromator and Photomultiplier

The light from the cassegrain telescope was focused onto the slit of a Czerny-Turner double monochromator (Spex Industries model 14018). This instrument consists of two basically identical grating dispersive sections coupled by two small mirrors and an auxiliary slit (see fig. 3.4). In each section, light from the object slit fills a 0.85 m focal length front surface f/8 primary mirror where it is collimated and redirected to an 1800 line/mm holographic grating mounted on a cosecant stepping motor drive; this drive is linear with wavenumber (reciprocal wavelength). The fundamental grating equation can be written as

$$m\,\lambda = d\,(\sin\alpha + \sin\beta)$$

where

λ = wavelength

figure 3.3

Spex Industries 1402 18 double monochromator.

M1,M2,M5,M6	0.85 m focal length spherical mirrors
G1,G2	1800 line/mm holographic gratings
S1,S2,S3	adjustable-width slits
P	RCA 31034 photomultiplier tube with Ga-As photocathode

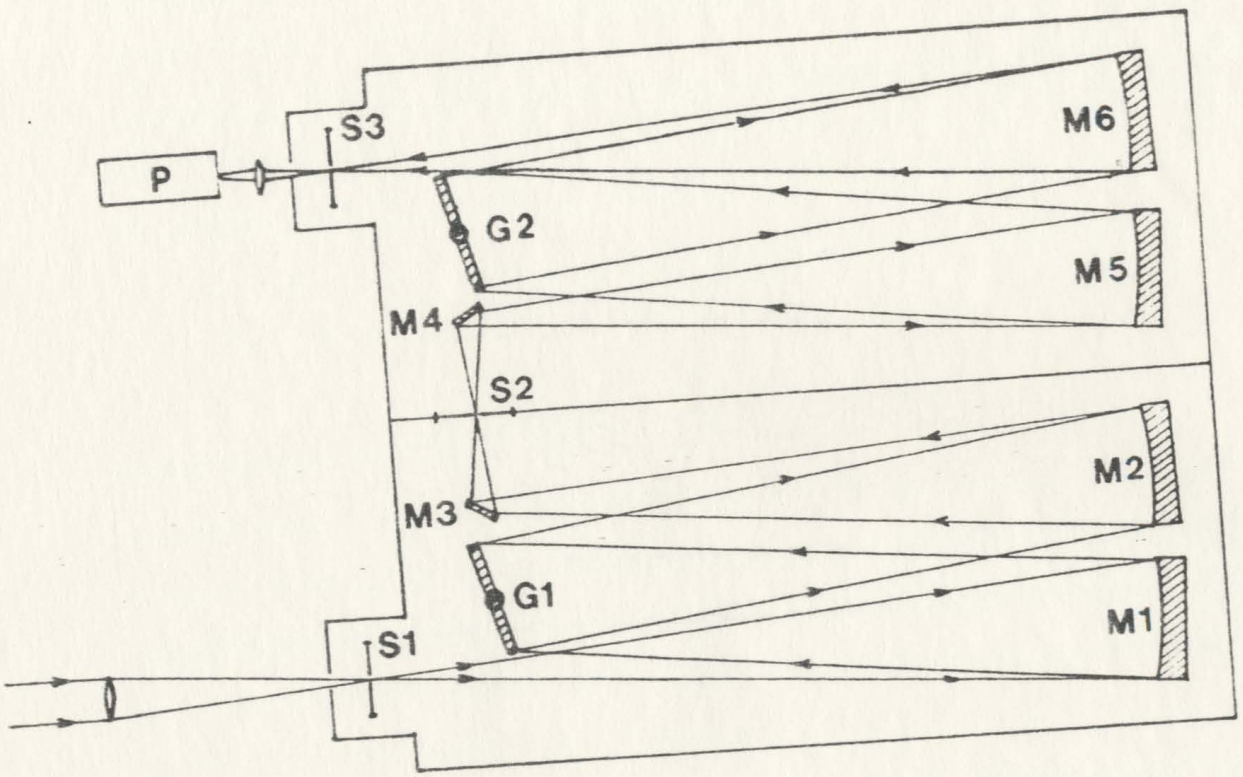
P
S3
M6
G2
M5
M4
S2
M2
M3
G1
M1
S1

m = diffraction order

d = grating spacing

α = the angle of incidence

β = the angle of diffraction

For the cosecant drive, $\alpha=\theta+\phi$ and $\beta=\theta-\phi$, where θ is the grating rotation measured from its position at the zeroth order and $\phi=6^{\circ}\ 15'$, so that

$$m\lambda = d\,(2\sin\theta\cos\phi)$$

The theoretical resolving power of such a mounted grating is simply

$$R_t = \frac{\lambda}{\delta\lambda}$$

$$= \frac{2W}{\lambda}\sin\theta\cos\phi$$

$$= mN$$

where W is the width of the grating, and N is the total number of rulings; for the gratings used, R_t is on the order of 180000. The effective resolution of the 14018 is stated as being 0.25 cm^{-1} at 632.8 nm for slit settings of 20-100-20 μm; typical slit settings used in this research were 300-300-300 μm and 400-400-400 μm, for an effective resolution of 4-5 cm^{-1}. This was sufficient for the present work, as the Raman feature widths averaged 20-30 cm^{-1}.

The first order reflection from the grating is collected by a second 0.85m mirror, and subsequently focused back down onto a transfer slit. In the second half of the monochromator, a similar slit opens to a small lens used to refocus the output onto the photocathode of the photomultiplier tube (RCA 31034) operating at 1750 volts potential. Thermionic emission and thus the dark count were kept low by cooling the tube in a thermoelectrically-cooled housing (Products For Research, Inc.) supplied with a steady 7 A current and connected to running tap water. The dark count was typically 5-10 counts/sec.

3.5 Electronics

The output from the photomultiplier tube was fed to an amplifier/discriminator (Princeton Applied Research model 1120) and the resulting signal passed to a photon counter set to accumulate counts over a preset period of time (Princeton Applied Research model 1109), usually 2 seconds. A linear analog voltage from the counter, a representation of the top three significant figures in the count, was fed to a strip chart recorder (Hewlet Packard 7133A) so that paper records of the spectra could be made, and simultaneously the count was also directed to a small digital tape drive (Techtran Industries, Inc. 816) at 300 baud for temporary storage before dumping the counts to a mainframe disk drive for processing with a VAX 8800. This operation was performed for individual spectra, as the tape drive had no means of distinguishing between two different records on the same cassette.

3.6 Sample Preparation

The CBS lipids used for this investigation were kindly provided by Joan M. Boggs of the Department of Clinical Biochemistry, The Hospital for Sick Children, University of Toronto, and were dispersed without further purification. The variants of CBS examined were those containing stearic acid (C18:0-CBS), hydroxy-stearic acid (C18:0h-CBS), lignoceric acid (C24:0-CBS), and hexacosanoic acid (C26:0-CBS). Other lipids used were all phosphatidyl cholines, and were provided by Kevin M. Keough of the Department of Biochemistry, Memorial University, also used without further purification; these were dipalmitoyl PC (DPPC), and 1-myristoyl-2-stearoyl PC (MSPC).

Capillary tubes to hold the lipid dispersions were fashioned from clean borosilicate dropping pipettes (Allied brand, Fisher Scientific) by first firing closed the small end of the pipette in a low flame and then cutting off this capillary section to a length of $\approx$45 mm. The typical inner diameter of a capillary was 1.0 mm, with a wall thickness of only 0.1 mm. No other intermediate glassware was used

in the sample preparation procedure, as the lipids were dispersed directly in the sample tubes.

Cation solutions for the CBS lipids were prepared from reagent-grade LiCl and KCl, using an analytical balance with a precision of 0.01 mg (Sartorius-Werke) to weigh known amounts of the salts into clean 15 ml vials, and adding 12.0 ml of triply-distilled H_2O. Cation solutions of 0.5 M and 2.0 M concentration of each of these salts were made. Measurements of the pH of these solutions were then made; the obtained pH values were 6.6±0.2 and 6.9±0.2 for 0.5 M KCl and LiCl respectively, and 6.3±0.2 and 5.9±0.2 for 2.0 M KCl and LiCl. The PC lipids were dispersed only in H_2O , which had a measured pH of 7.5±0.2. As discussed below, the lipids were dispersed in small diameter capillaries; this precluded direct pH measurements of the samples.

To prepare a dispersion, the empty capillary was first weighed and the weight recorded. Then approximately 1.5 mg - 2.0 mg of dry lipid powder was loaded into the top of the tube and gently pulled into the bottom by tapping the capillary on the lab benchtop, and the capillary again weighed. Using a 25 μl syringe, 10 μl of cation-solution was then transferred into the tube, shaken down onto the lipid, the tube weighed again, and then using a clean stainless steel wire the lipid and solution were mixed together at room temperature. After a final weighing, the capillary tube was sealed at the top in a low burner flame, and then the coarse dispersion brought to 90° C+ by immersing the lower half of the tube in an ultrasonic water bath for 3 to 5 minutes, all the while intermittently mixing the dispersion by flicking the tube gently with a finger. Following this operation, the capillary was placed in a benchtop centrifuge (International Equipment Co. model CL) and centrifuged at high speed for 1 to 2 hours in order to separate the dispersion from the excess aqueous phase in the tube. The appearance of the dispersion was that of a thick, white mass not unlike cream, with a well-defined boundary between the dispersion and the layer of cation solution sitting above it. Heating the dispersion to above ≈80° C for an hour or more seemed to cause it to pull away from the side of the capillary tube and compress

slightly; in many cases the dispersion tended to float in the excess aqueous phase. Once made, most of the lipid dispersions were stored at -10^{o} C in a block of Styrofoam in a freezer. A few of the initial 0.5 M cation samples were stored at room temperature. To remove the effects of prolonged storage at these temperatures, the dispersions were heated to 90^{o} C+, above their main transition temperatures, in a water bath for 2-5 minutes immediately prior to their insertion into the sample holder, usually at 10^{o} C at the beginning of a run.

3.7 Data Collection

The vibrational spectra of lipids encompasses a large range, from 100 cm^{-1} for the acoustical modes up to 2800-3100 cm^{-1} for the C-H stretching modes. Because many such spectra were required to be collected contiguously within certain time constraints, Raman spectra were normally obtained only over the shorter C-H stretching region or, more rarely, over the optical modes at 1000-1150 cm^{-1}. Survey spectra required scanning across the entire 3000 cm^{-1} field.

The Raman spectra were obtained at a scanning rate of 0.5 cm^{-1}/s, with the photon counter set to accumulate counts over a 2 sec period so that the spectra were recorded at one datum per cm^{-1}. A typical run over the stretching mode region started at 2700 cm^{-1} and continued up to 3200 cm^{-1}, taking some 17 minutes. A run was made only after the temperature of the sample holder had stabilized for at least 2 minutes; it took an additional 4 minutes to scan up to the first Raman feature, so that an equilibriation time of at least 6 minutes was given the lipid sample for each run. The starting and stopping of a run was performed manually; the tape drive write enable switch and Spex drive enable switch were toggled simultaneously, and the pen on the strip chart was lowered or raised after this. Upon finishing a scan, the sample cell temperature was then set in preparation for the next run, and the data stored digitally on tape was dumped to the VAX while the cell came up to temperature. Typically, the increase in temperature took about one minute per degree for either circulating bath used; where many spectra were collected to obtain a temperature profile, this was usually

done by heating between runs. Runs comprising a temperature profile were started at about 10° C and ended between 70 and 90° C.

3.8 Data Reduction

Once stored on disk for access by the VAX, the lipid C-H stretching mode spectra were analyzed by a compiled Basic program written primarily to subtract from the data a large background feature sitting at about 2900–3200 cm^{-1}, due most probably to O-H stretching associated with the CBS headgroup-water interaction (for a listing, see Appendix 1). This feature was present in in the spectra of PC dispersions, though at a much reduced magnitude.

Briefly, the program loaded in four numbers included at the top of a data file when it was created that described the Spex scanning speed, the count integration time, the starting wavenumber, and the thermistor resistance, and then loaded in the raw counting data. If it encountered any illegal entries in the data due to the occasional bit error, the program substituted the bad datum with the previous point. It then calculated the sample temperature, and smoothed the data using a simple averaging procedure;

$$y'(j) = \sum_{i=-\frac{n-1}{2}}^{\frac{n-1}{2}} \frac{y(j-i)}{n}$$

over all j, where j is equal to the wavenumber corresponding to the spectral intensity y(j) minus the first wavenumber of the spectrum, and n is 1,3,5, or 7. Sampling the data from 2700 to 2825 cm^{-1}, and 3050 cm^{-1} to the end of file, the program then attempted to fit a Maclauren series to the background function using a least squares technique;

$$f(x) = \sum_{m=0}^{\infty} a_m \frac{(x-x_o)^m}{m!}$$

Here the series was truncated to m=4, x_o was made approximately equal to zero by shifting the data to be fitted to 3000 cm^{-1}, and the data were divided by 1000

to prevent an overflow on the VAX. This background function was subtracted from the smoothed data.

Two order parameters were then determined. The location of the ≈2845, ≈2885, and ≈2935 cm^{-1} Raman features were found, and the ratios $\frac{I_{2850}}{I_{2885}}$ and $\frac{I_{2935}}{I_{2885}}$ calculated; the intensities here are simply the Raman peak heights at the associated wavenumbers with respect to the baseline. As the data are counts of photon detection events per unit time, Poisson statistics can be applied to determine the errors in these ratios. For each peak, the error after smoothing is simply

$$\Delta y_p = \sqrt{\frac{y_p}{n}}$$

where y_p is the photon count for the peak before the background was subtracted. The ratio is expressed as

$$R = \frac{y_1}{y_2} \pm \sqrt{\left(\frac{\Delta y_1}{y_1}\right)^2 + \left(\frac{\Delta y_2}{y_2}\right)^2}$$

and the spectrum displayed using calls to Tektronix Plot 10 TCS subroutines. Typical errors were in the order of 3-5% (see fig. 3.4).

Phase transition temperatures were obtained from the thermal profiles generated when the two collections of order parameters from a series of Raman spectrum runs were plotted against temperature. The solid curves drawn were not mathematical fits, but were rendered by eye to be indicators of the trends in the data. Typically the transition manifested itself as an abrupt increase in the value of a parameter over a small temperature range; the temperature at the mid-point of this rise is quoted as the transition temperature, and is determined graphically by extending the order parameter versus temperature curve on either side of the transition past its adjacent inflection point, and constructing a vertical line between these two limits that intersects the experimental curve midway. The

figure 3.4

Raman spectrum of C18:0-CBS in 2 M Li^+ at 20° C,

a) before, and

b) after smoothing the data and subtracting a fitted background profile.

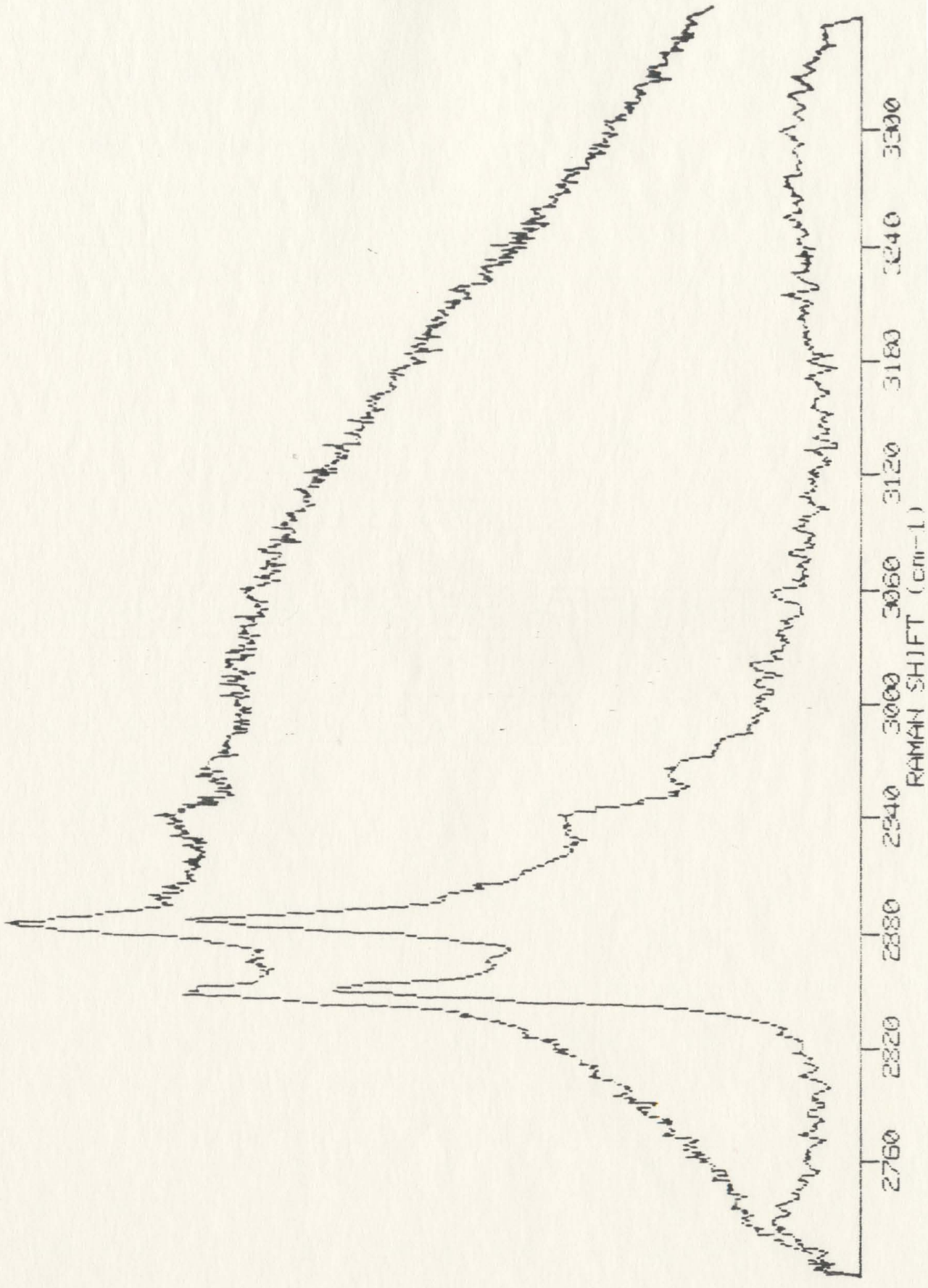
2760
2820
2880
2940
3000
3060
3120
3180
3240
3300
RAMAN SHIFT (cm-1)

temperature at which this vertical line rests is taken as the transition temperature, and the length of the line between the limits is taken as being the magnitude of change in the associated order parameter through the transition. This graphical analysis procedure is illustrated in a set of test profiles generated from a series of runs run of a DPPC/H_2O system, presented in the following chapter (fig. 4.2). A short program was written to display both profiles for a given set of Raman spectra on a single set of axes, and a listing of this routine is presented in Appendix 2.

CHAPTER 4. RESULTS AND DISCUSSION

In this work bilayer systems of various species of cerebroside sulphate (CBS) in aqueous cation solutions were examined, as previously described. By using species of CBS with varying chain-length asymmetry, in this case the fatty acid chain being 18, 24, or 26 carbons in length as compared with the effective 14 carbon chain length of the sphingosine base, the effect of asymmetry on the probability of interdigitated chain packing was observed. Expected to be even more pronounced than the effect of the chain lengths were the various interactions due to the negatively-charged headgroups. With this in mind, each CBS species was examined in the presence of two cations of differing hydrated ionic size, Li^+ and K^+, usually at a concentration of 2 M but in a few cases at one quarter of this. The aim here was to determine the kinds of effects the resulting shielding of the sulphate charge produced. These concentrations and cations were chosen specifically to match those used by Boggs *et.al.* in their recent studies of CBS using DSC and ESR [26-28]. CBS, having an amide group (NH) and many hydroxyl groups (OH) associated with both the sugar-ring and the interfacial region of the lipid, is thought to interact strongly with the aqueous phase and neighboring lipid molecules though hydrogen bonding. This effect is also studied by investigating a variant of the 18-carbon acyl chain species of CBS (C18:0-CBS) with one additional hydroxyl group attached to this chain (C18:0h-CBS).

A series of some C-H stretching region Raman spectra collected with increasing temperatures for a dispersion of C18:0-CBS in 2 M $K^+$is illustrated in fig. 4.1. The various changes in the spectral contour with changes in the sample temperature, as noted earlier, are clearly evident especially when the lipid chains develop *gauche*-conformers as the bilayers in the dispersion make the transition to the fluid phase. The temperature profiles for this system and the others investigated

figure 4.1

Several Raman spectra of C18:0-CBS in 2 M K^+ at different temperatures, illustrating the changes in the C-H stretch vibrational modes as the chains develop *gauche* -conformers.

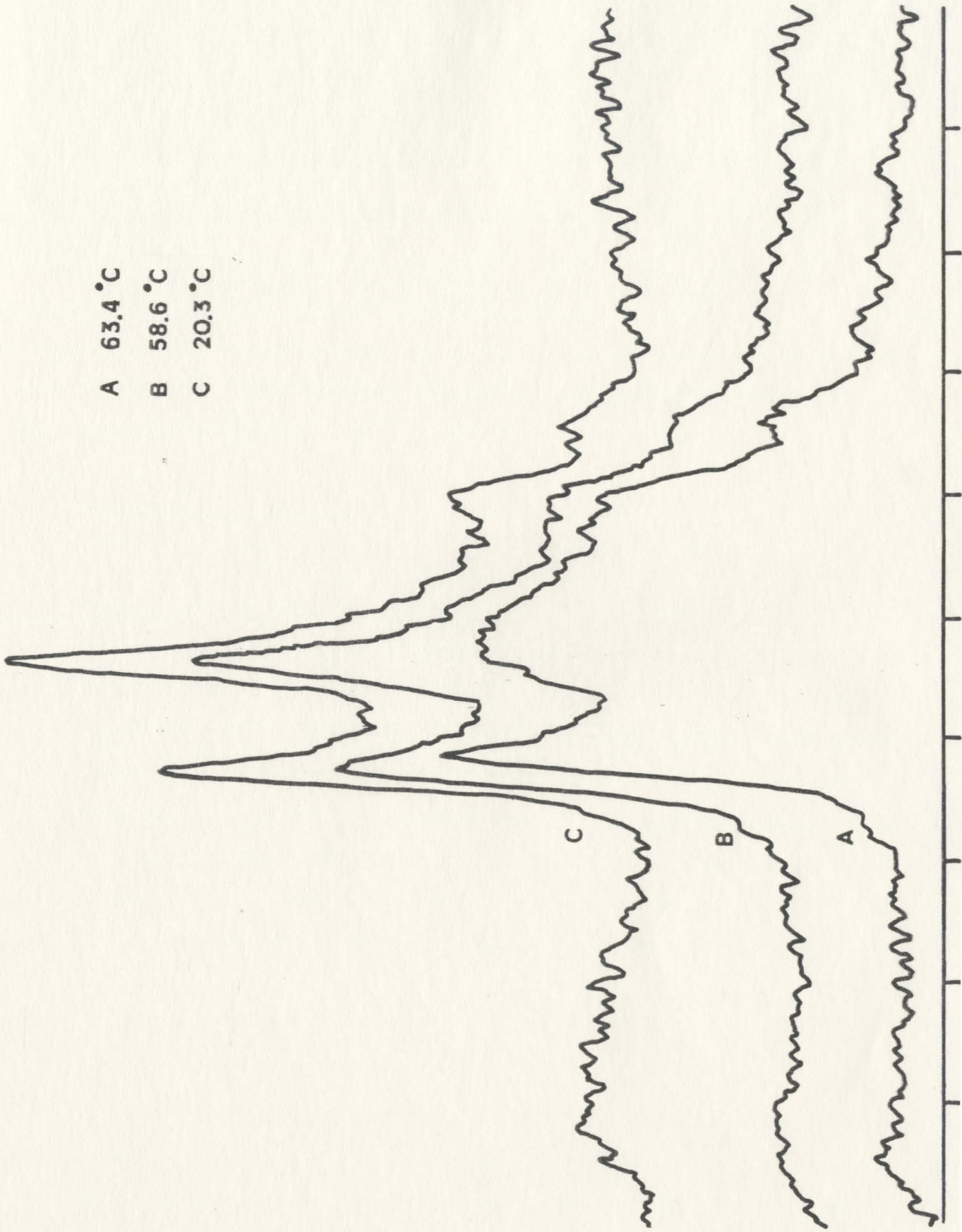
A 63.4 °C
B 58.6 °C
C 20.3 °C
C
B
A

are presented in figures 4.4 to 4.11 for the 2 molar cation dispersions of the three non-hydroxylated CBS species, in figures 4.12 to 4.14 for C18:0-CBS in 0.5 M Li^+ and C26:0-CBS in 0.5 M Li^+ and K^+ respectively, and in figures 4.15 and 4.16 for C18:0h-CBS in 2 M K^+ and 0.5 M Li^+ respectively. The upper curve in each figure reflects changes in the spectral parameter $R_2 = \frac{I_{2845}}{I_{2885}}$ (Δ), and the lower curve reflects changes in $R_1 = \frac{I_{2935}}{I_{2885}}$ (O) as the sample temperature is increased. No spectra were collected where the temperature of the sample was gradually *decreased* in small increments. The relevant data drawn from these profiles are presented in table 4.1.

4.1 DPPC and MSPC

As a basis for comparing values of R_1 and R_2 obtained for CBS, and as a test of the procedures and apparatus used in this study, thermal profiles of dispersions of dipalmitoyl phosphatidyl choline (DPPC) and 1-myristoyl 2-stearoyl phosphatidyl choline in excess H_2O were generated, and are presented in figures 4.2 and 4.3 respectively. The profile for DPPC matches similar profiles obtained for this well-characterized system elsewhere [eg.,12], and the obtained value for T_m of 41.1° C is the accepted value both by DSC and previous Raman investigations. The profiles for MSPC are far too flat and broad to use as a comparison, probably owing to insufficient evaporation of the solvent in which the lipid was stored prior to dispersion in the H_2O, and are included only for completeness.

4.2 C18:0-CBS in 2M Li^+

Two sets of data for C18:0-CBS in 2M Li^+, one for a dispersion stored at −10° C (as were most of the 2M cation solution samples in this study), and one for a dispersion stored at room temperature, about 20±2° C, are presented in figures 4.4 and 4.5 respectively. The principal purpose of testing storage effects,

Table 4.1 Thermal Profile Data

system	$T_m(R_1)$	$T_m(R_2)$	R_1[a]	R_2[a]	ΔR_1	ΔR_2	
C18:0-CBS + 2M K^+[b]	65° C	64° C	0.30	0.70	0.44	0.28	sharp
C18:0-CBS + 2M Li^+[b]	48	49	0.28	0.75	0.33	0.21	sharp
C18:0-CBS + 2M K^+	(53),60	60	0.33	0.75	(0.06),0.33	0.27	sharp
C18:0-CBS + 2M Li^+	50	51	0.42	0.75	0.38	0.25	med. sharp
C24:0-CBS + 2M K^+	40,62	40,59	0.33,0.41	0.72,0.83	0.07,0.19	-	sharp in R_1
C24:0-CBS + 2M Li^+	52	54	0.34	0.72	0.29	0.28	broad
C26:0-CBS + 2M K^+	57	55	0.39	0.82	0.30	0.22	broad
C26:0-CBS + 2M Li^+	54	52	0.33	0.71	0.27	0.29	broad
C18:0-CBS + 0.5M Li^+	54	53	0.28	0.61	0.26	0.19	sharp
C26:0-CBS + 0.5M K^+	63	63	0.30	0.73	0.38	0.19	broad
C26:0-CBS + 0.5M Li^+	52	51	0.27	0.49	0.38	0.43	sharp
C18:0h-CBS + 2M K^+[c]	≈75?	≈75?	0.6	0.9	-	-	-
C18:0h-CBS + 0.5M Li^+	53	53	0.36	0.71	0.18	0.14	sharp
DPPC + H_2O	41	41	0.33	0.74	0.33	0.18	sharp
MSPC + H_2O	46	-	0.40	-	0.25	-	broad

[a] 20° C below T_m

[b] sample stored at ambient room temperature (20° C).

[c] large scatter in the data; mostly indeterminate.

figures 4.2, 4.3

Temperature profiles for DPPC and MSPC, respectively, in water. The upper curve (Δ) is derived from the Raman feature intensity ratio $\frac{I_{2845}}{I_{2885}}$ and the lower curve (O) is derived from the ratio $\frac{I_{2935}}{I_{2885}}$.

fig. 4.2

DPPC + H_2O

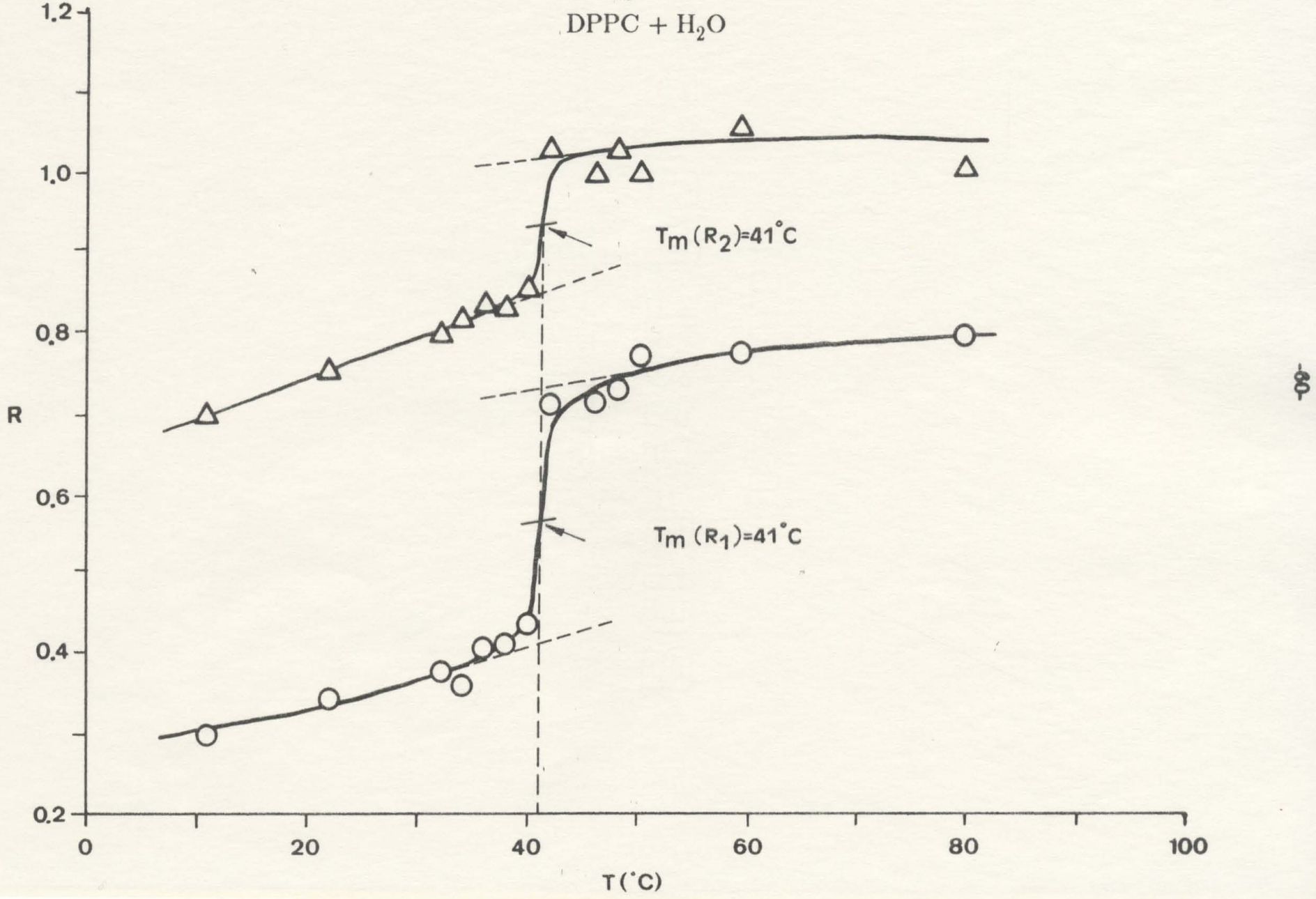

fig. 4.3

MSPC + H_2O

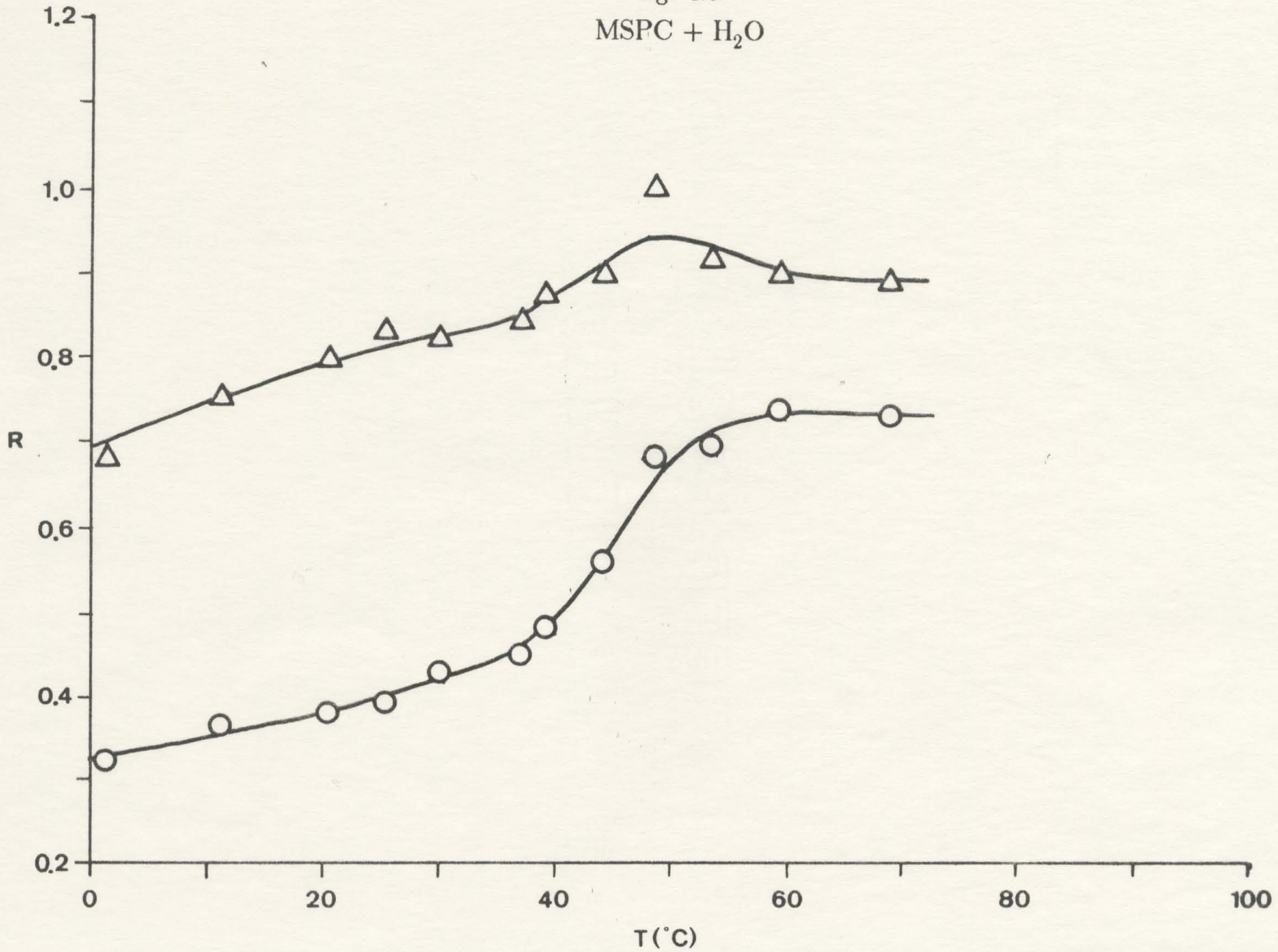

even though the samples had all been heated to above their main transition temperatures for 2-5 minutes, was to assess the validity of their comparison with the few 0.5 M cation dispersions which were previously investigated in the present study, and which had not been stored in a freezer.

The cold-stored dispersion shows a sharp transition at 50 and 51° C in the R_1 and R_2 data, respectively. The relative change in the disorder in the lipid chain packing through the transition is comparable to values obtained in a similar way for DPPC, ΔR_1 being 0.38 as opposed to 0.33 and ΔR_2 being 0.25 as opposed to 0.18.

Values for R_2 at 20° C below T_m are nearly identical to those for DPPC; R_2=0.74 for this sample compared to 0.75 for DPPC, whereas C18:0-CBS in 2 M Li^+ seems to exhibit a greater tendency to disorder at lower temperatures in the R_1 data than does DPPC.

The temperature profiles for this dispersion after being stored at ambient temperature are similar (fig. 4.5). The R_2 profile is nearly identical to that in the cold-stored case in fig. 4.4, having a slightly lower T_m of 49° C. T_m in the R_1 data was 48° C, and ΔR_1 is comparable to its value in the former case, but the entire R_1 profile appears to be shifted downwards with respect to the former profile. As this shift does not occur in the R_2 profile a systematic error involving the removal of the large background feature present in all of the CBS spectra collected might be expected. This unfortunate possibility arises from the sheer difficulty in removing the background, and supports the need for the redundancy obtained by choosing to derive two spectral parameters for Raman features whose intensity-versus-temperature behavior is derived from similar mechanisms.

4.3 C18:0-CBS in 2 M K^+

Again, two sets of profiles were obtained for C18:0-CBS dispersions stored at -10 and 20° C, but this time for the lipid in the presence of 2 M K^+ (fig. 4.6, 4.7). For the cold-stored sample T_m = 60° C in both the R_1 and R_2 profiles; there

appears to be a slight indication of a pre-transition at 53° C in the R_1 data, but this is not seen in the upper curve. The transition is sharp and of a similar magnitude as that for the 2 M Li^+-buffered samples of this CBS species, and the relatively temperature-insensitive nature of both R_1 and R_2 is also shared between the samples as contrasted with the simpler DPPC system. T_m is $\approx$10° C higher in 2 M K^+ than in 2 M Li^+ as obtained here.

Generally, the R_1 and R_2 profiles seen in fig. 4.7 were very similar to those in fig. 4.6, except that upon closer inspection the ambient-stored R_2 profile is on the whole shifted to slightly higher disorder with respect to the curve in fig. 4.6, while the R_1 profiles are this time very close. The temperature of the single phase transition is $T_m = 65$ and 64° C for the R_1 and R_2 data respectively, which is slightly higher than in fig. 4.6. It might be suggested that in addition to a small systematic error present in one of the sets of reduced Raman spectra the bilayers in the ambient-stored sample appear to be genuinely more ordered which would follow from the small increase in T_m seen both in the R_1 and R_2 profiles. The presence of differences for whatever reason between the two sets of profiles forces a certain amount of caution when interpreting the results of the few 0.5 M cation dispersions studied; this will be discussed later.

J. Boggs *et.al.* have obtained various transition temperatures for C18:0-CBS both in 2 M K^+ and 2 M Li^+ using DSC techniques [26,27]. Their results, obtained with both heating and cooling runs at 10° C/min. and corrected for instrumental hysteresis, show one or more smaller-enthalpy events in addition to the main feature, ascribed to the transition to the fluid phase, for all CBS species. These smaller peaks correspond to phase transitions not seen in the present data; most of them are described by these researchers as metastable, and are strongly dependent on the sample preparation and history. Comparing their values for the principal transition temperature T_m for heating runs only of C18:0-CBS, they found T_m =63.9 and 51.4° C for 2 M K^+ and Li^+ buffers respectively, with which the values reported here for both the cold- and ambient-stored samples of

these systems agree fairly well. Overall, the data presented here do not seem to indicate interdigitated packing in bilayers of C18:0-CBS under the conditions employed.

4.4 C24:0-CBS in 2 M Li^+

Unlike the nearly-symmetric C18:0-CBS, this lipid was expected to exhibit interdigitated packing effects which would be evident if more than just the chain melting transition was observed. As seen in fig. 4.8, only a single broad transition occurring at $T_m = 52$ and 54^o C for the R_1 and R_2 profiles, respectively, takes place for bilayers of this species of CBS in the presence of 2 M Li^+. These temperatures are comparable to those obtained for the shorter acyl chain C18:0-CBS in the same buffer. For reference, the R_1 profile is similar to that in fig. 4.1 for DPPC. The R_2 profile is largely temperature-insensitive below about 40^o C. This contrasts with finite slope of DPPC's R_2 curve. A possible explanation for the broadness of the transition might be that at this temperature islands of lipid in the bilayer begin to adopt a different (interdigitated) packing arrangement, but that headgroup interactions are such that those transitions are not very cooperative and thus these altered-phase islands tend to remain isolated. Caution should be exercised here, as by itself this interpretation violates the equilibrium phase rule and so to be viable other factors or non-equilibrium conditions must be involved.

4.5 C24:0-CBS in 2 M K^+

A change in the chain ordering associated with a change in the packing arrangement of the lipid chains is seen at 40^o C in both temperature profiles for C24:0-CBS in the presence of 2 M K^+ as presented in fig. 4.9. The main transition occurs at 62 and 59^o C in the R_1 and R_2 data respectively, again about the same as for C18:0-CBS in 2 M K^+ despite the longer acyl chain. The profiles are of near-zero slope below each of the two phase transitions, again in contrast to DPPC whose acyl chains do not interdigitate in bilayers to any appreciable

extent. ΔR_1=0.07 and ΔR_2=0.08 across T_m, in comparison with these values for the main lipid chain melting event where ΔR_1=0.19; oddly, this transition as seen in the upper profile is marked by an abrupt increase in the rate of disordering as opposed to the disordering itself. The slope of this curve above T_m is the same as that for the R_1 profile, but has no ordering change at T_m unlike that latter curve. It seems that at least for this system there is an abrupt increase in the vibrational coupling between the terminal CH_3 and predominating CH_2 groups in the chains without an abrupt decrease in the interchain CH_2-CH_2 mode coupling at T_m, and that after this temperature only the latter coupling changes, at a steady rate.

This behavior below the second (main) transition, T_{m_2} is strikingly similar to that observed for the 24-carbon acyl chain sphingomyelin/H_2O system investigated by Levin *et.al.* [24], whose interpretation of the smaller transition was that the bilayers went from a mixed interdigitated phase to a partially interdigitated one as described in the Introduction. They found R_1 to change from 0.31 to 0.42 at 48.5° C and then to 0.78 at 54.5° C with no significant slope in the profile between these transitions. Their R_2 data behaved similarly. In comparison, for C24:0-CBS in K^+, R_1 changes from 0.33 to 0.44 at 40° C and then to 0.65 at 62° C. This correlation would be expected if the K^+ in the buffer almost totally shielded the negative charge in the sulphate of the CBS headgroups, virtually removing the interheadgroup repulsion due to this charge making the resulting CBS system much more like the SPM system. Owing to the similarity of the two data sets, Levin *et.al.* 's interpretation is adopted here as well, meaning that evidence of interdigitated packing is seen implicitly in 2 M K^+ but not in 2 M Li^+ for C24:0-CBS.

Again a comparison of these results are made with the calorimetry data of Boggs. For C24:0-CBS they found that T_m=69.0 and 55.6° C in 2 M K^+ and Li^+ respectively, heating at 10° C/min. Upon cooling from the fluid phase these temperatures were 54.9 and 43.1° C respectively, indicating a large degree of sample

hysteresis (as before, their values for T_m are corrected for instrumental hysteresis). The values reported in the current study lie between these warming and cooling values. Metastability is not seen.

4.6 C26:0-CBS in 2 M Li^+

The two temperature profiles for the 26-carbon acyl chain species of CBS in the presence of 2 M Li^+ is virtually indistinguishable from that of the 24-carbon acyl chain species (fig. 4.10). There is no explicit evidence of a pre-transition between gel states of different, probably interdigitated, phases but the same single, broad transition seen in fig. 4.8. This behavior would be expected to some degree as the two species are very similar, differing in only two methylene units in the acyl chain. However, the transition temperature itself, 54 and 52° C in the R_1 and R_2 curves respectively, are also identical to that for C24:0-CBS in 2 M Li^+. It would appear that unlike for the case of simpler phospholipids such as DPPC and others, T_m is determined more by headgroup interactions than hydrocarbon chain lengths.

4.7 C26:0-CBS in 2 M K^+

Following from the above results, we would expect to see evidence of interdigitation in this system as in C24:0-CBS in the presence of 2 M K^+. In this case, however, such behavior is not clearly seen (fig. 4.11). Although there is a hint of a change in the temperature sensitivity of the hydrocarbon chain ordering at about 30–40° C in both the R_1 and R_2 data, this evidence is not compelling. Subsequent series of spectra collected to generated new profiles for this system were of no additional aid in clarifying this observation as these profiles suffered an even greater data spread. Transition temperatures of 57 and 55° C in the lower and upper curves respectively are also somewhat lower than for C24:0-CBS and C18:0-CBS in this cation at this concentration, though still marginally higher than T_m in 2 M Li^+.

figures 4.4-4.11

Temperature profiles generated from Raman data for various species of non-hydroxylated CBS in 2 M cation solutions.

fig. 4.4

C18:0-CBS + 2.0 M Li^+

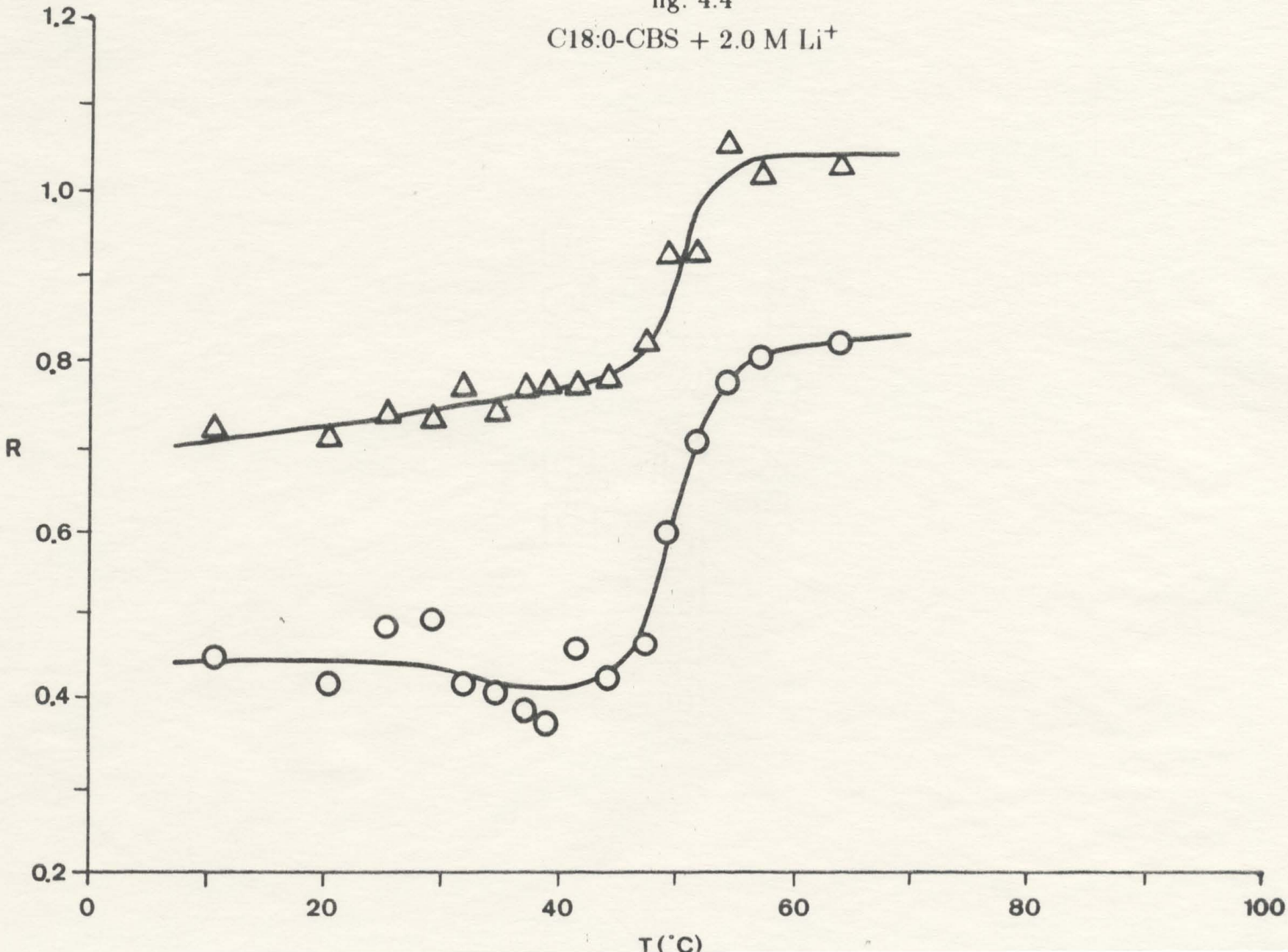

fig. 4.5

C18:0-CBS + 2.0 M Li^+

(stored at 20° C)

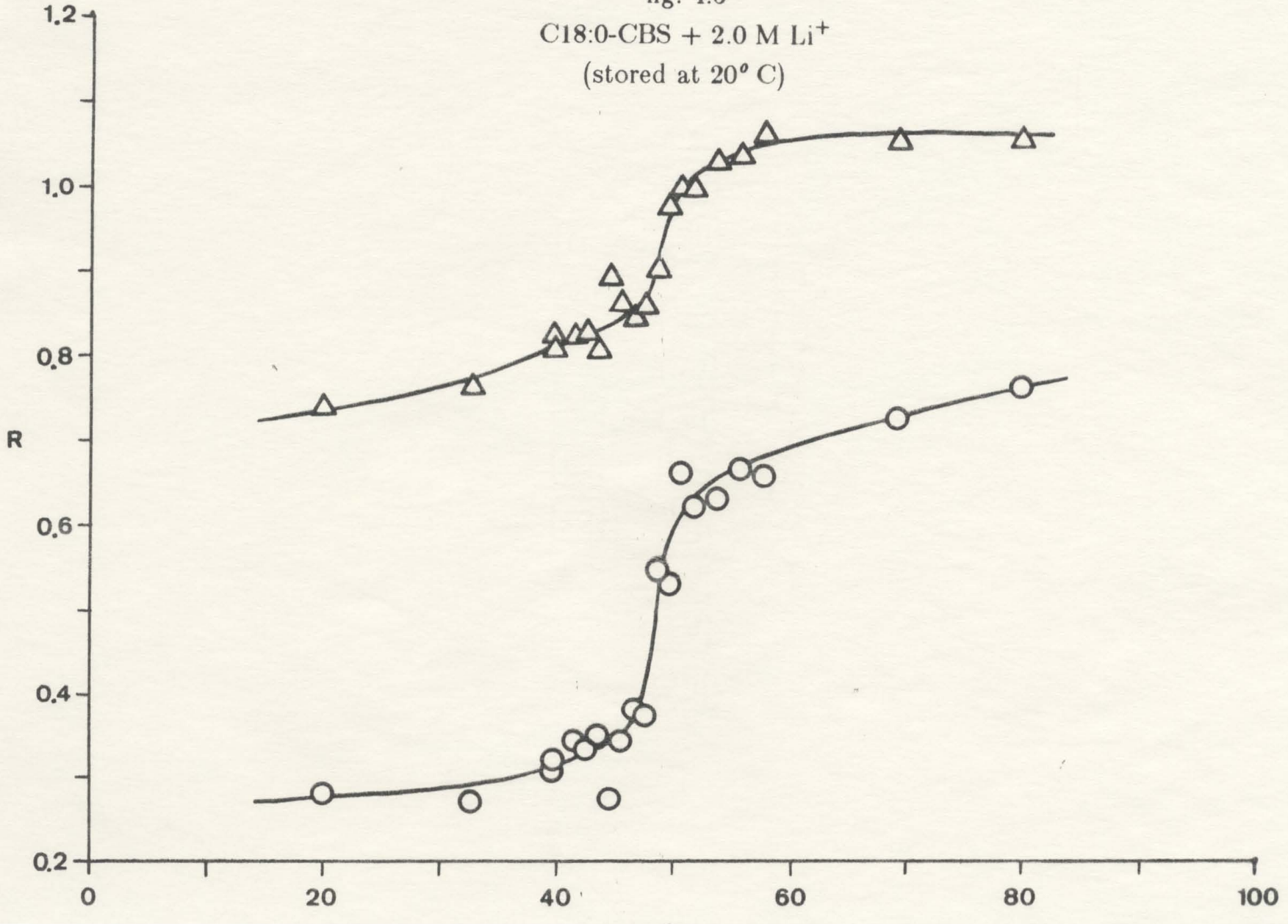

fig. 4.6

C18:0-CBS + 2.0 M K^+

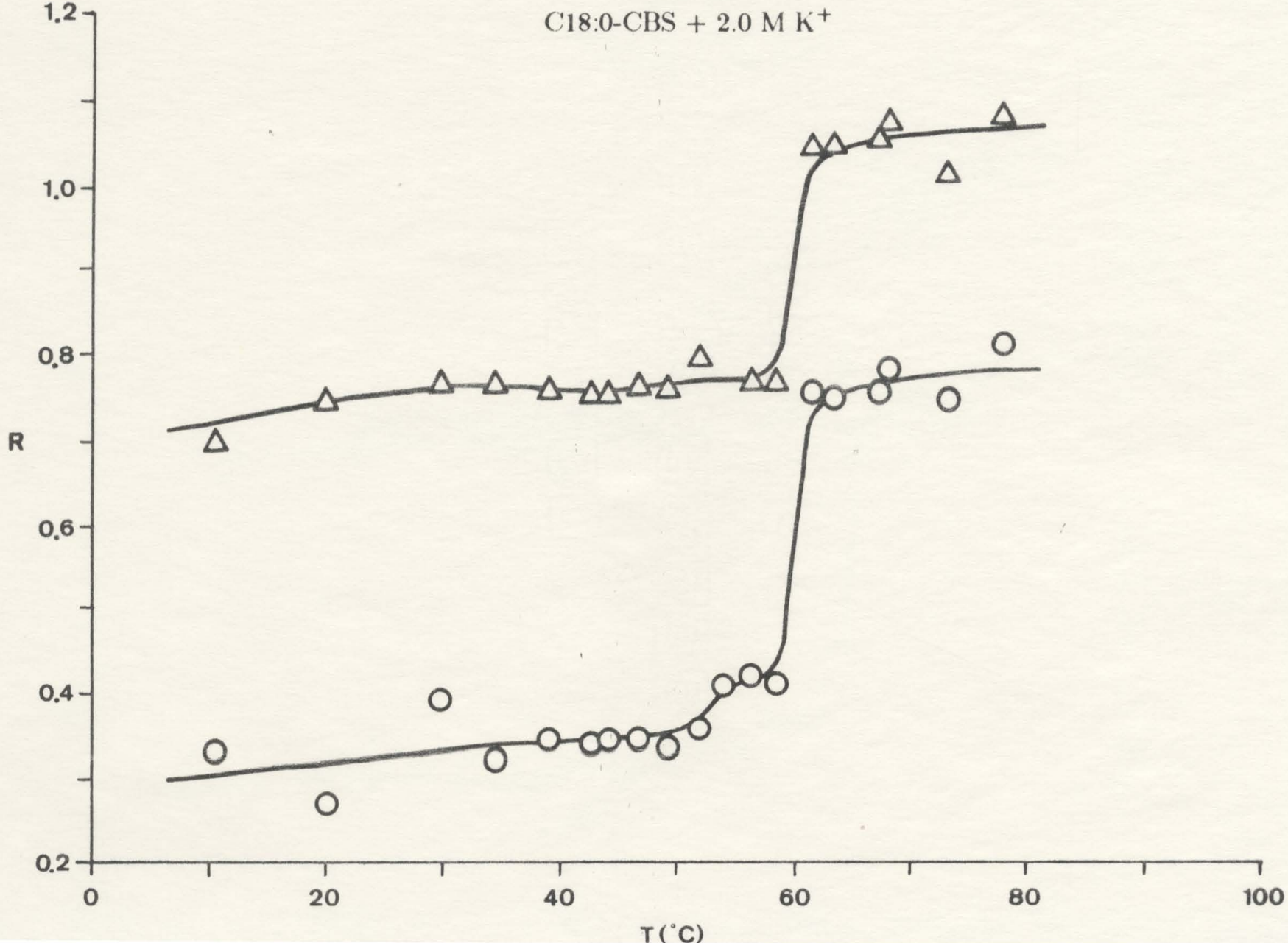

fig. 4.7

C18:0-CBS + 2.0 M K^+

(stored at 20° C)

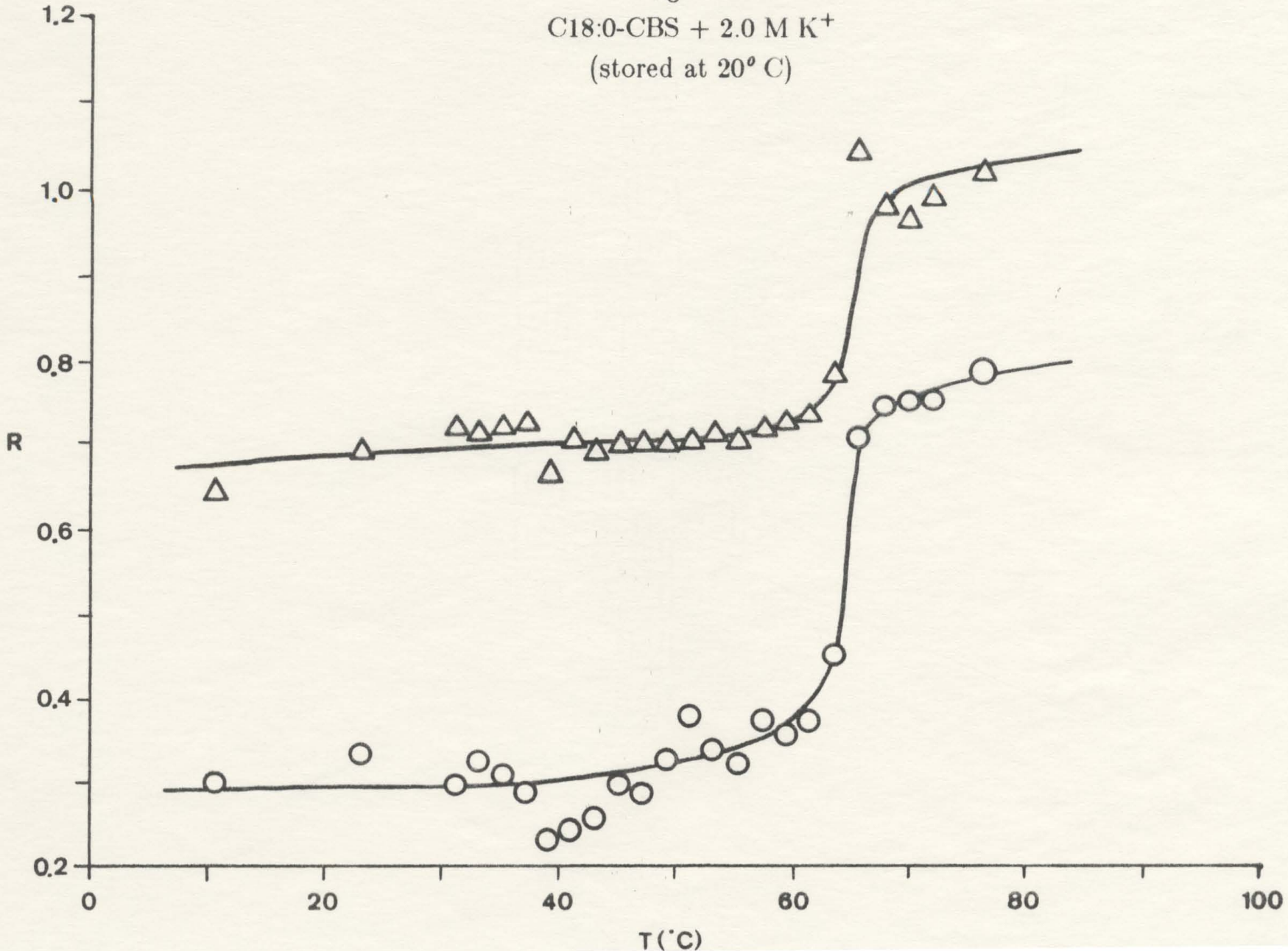

fig. 4.8

C24:0-CBS + 2.0 M Li^+

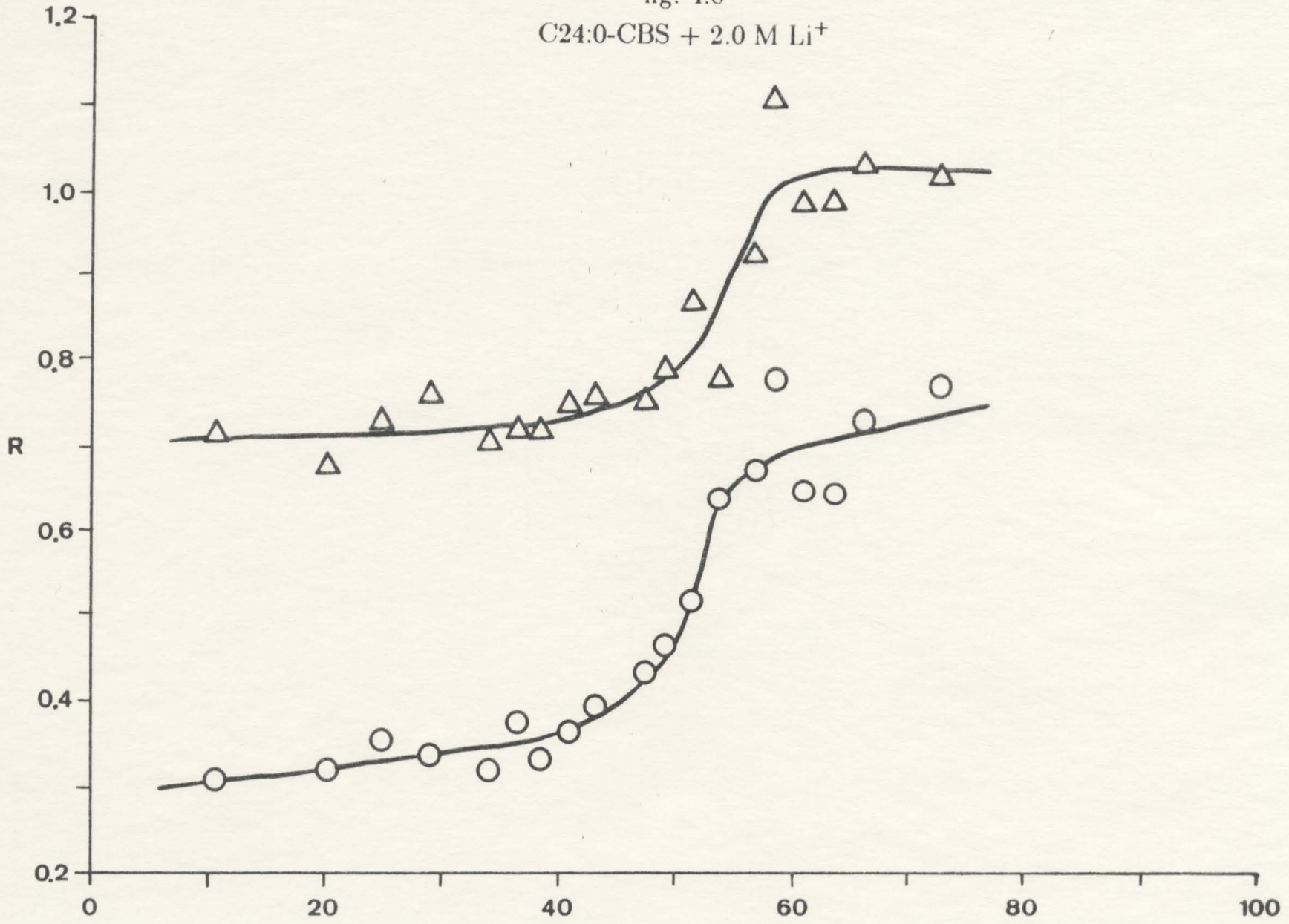

fig. 4.9

C24:0-CBS + 2.0 M K^+

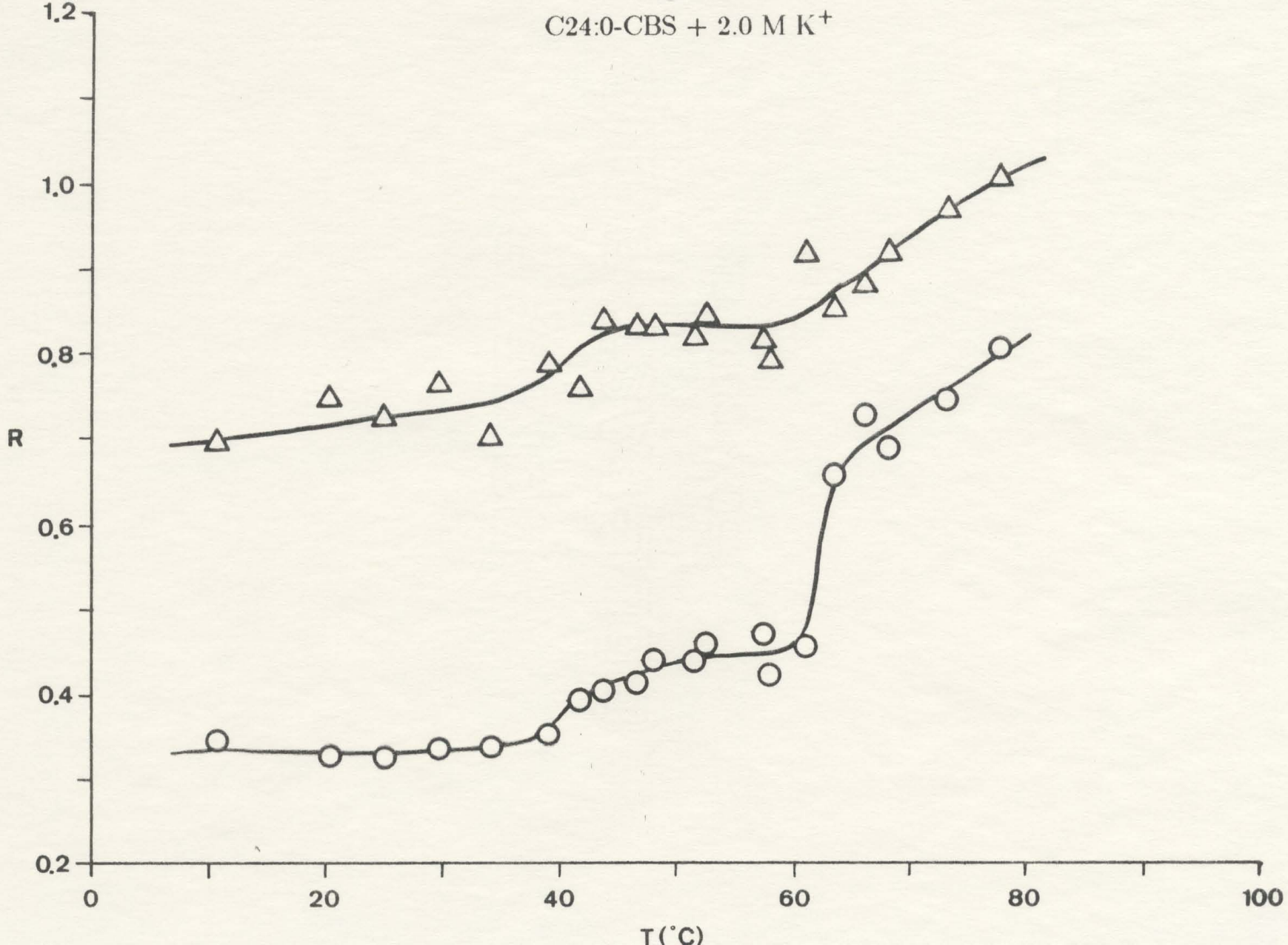

fig. 4.10

C26:0-CBS + 2.0 M Li^+

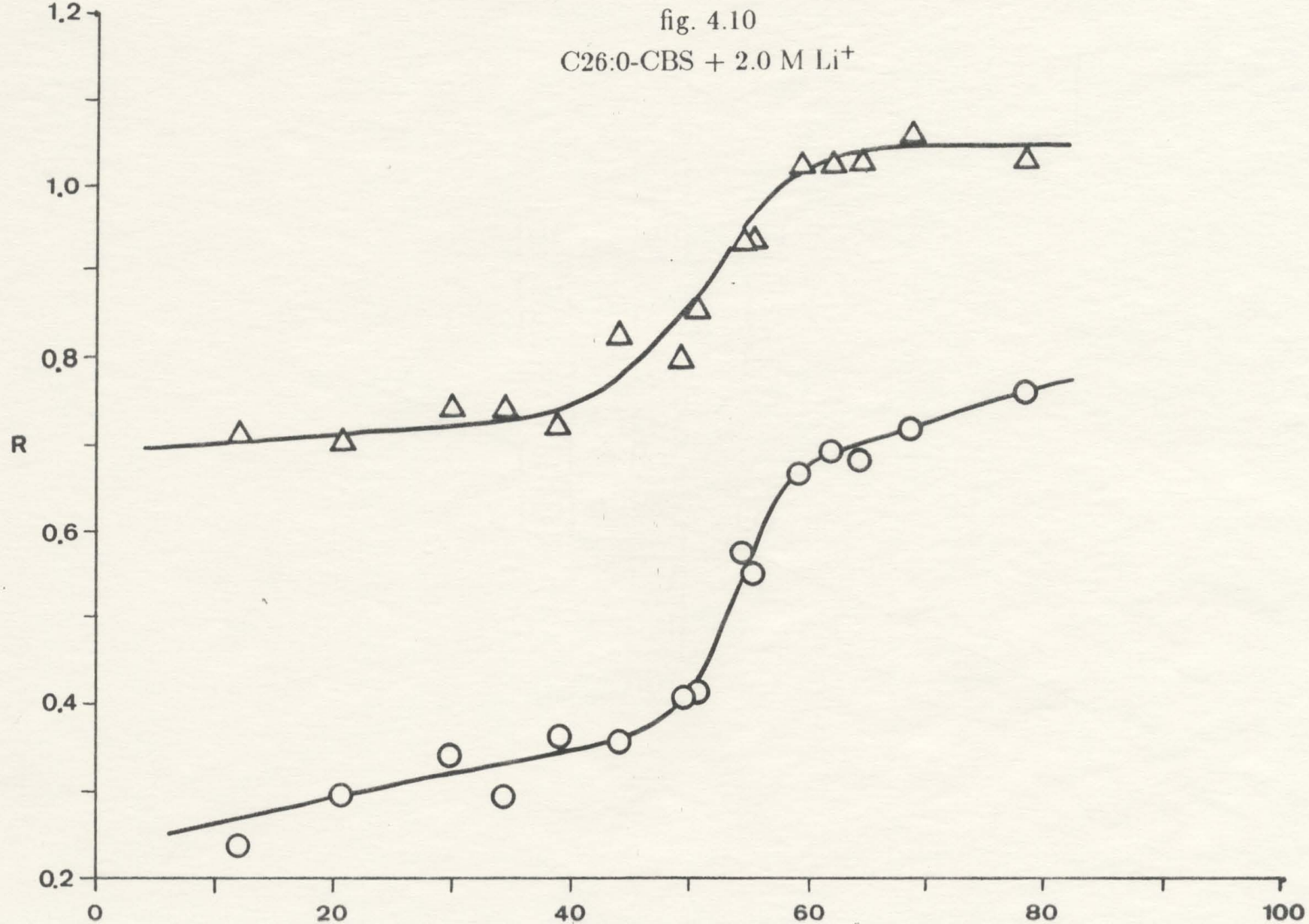

fig 4.11

C26:0-CBS + 2.0 M K^+

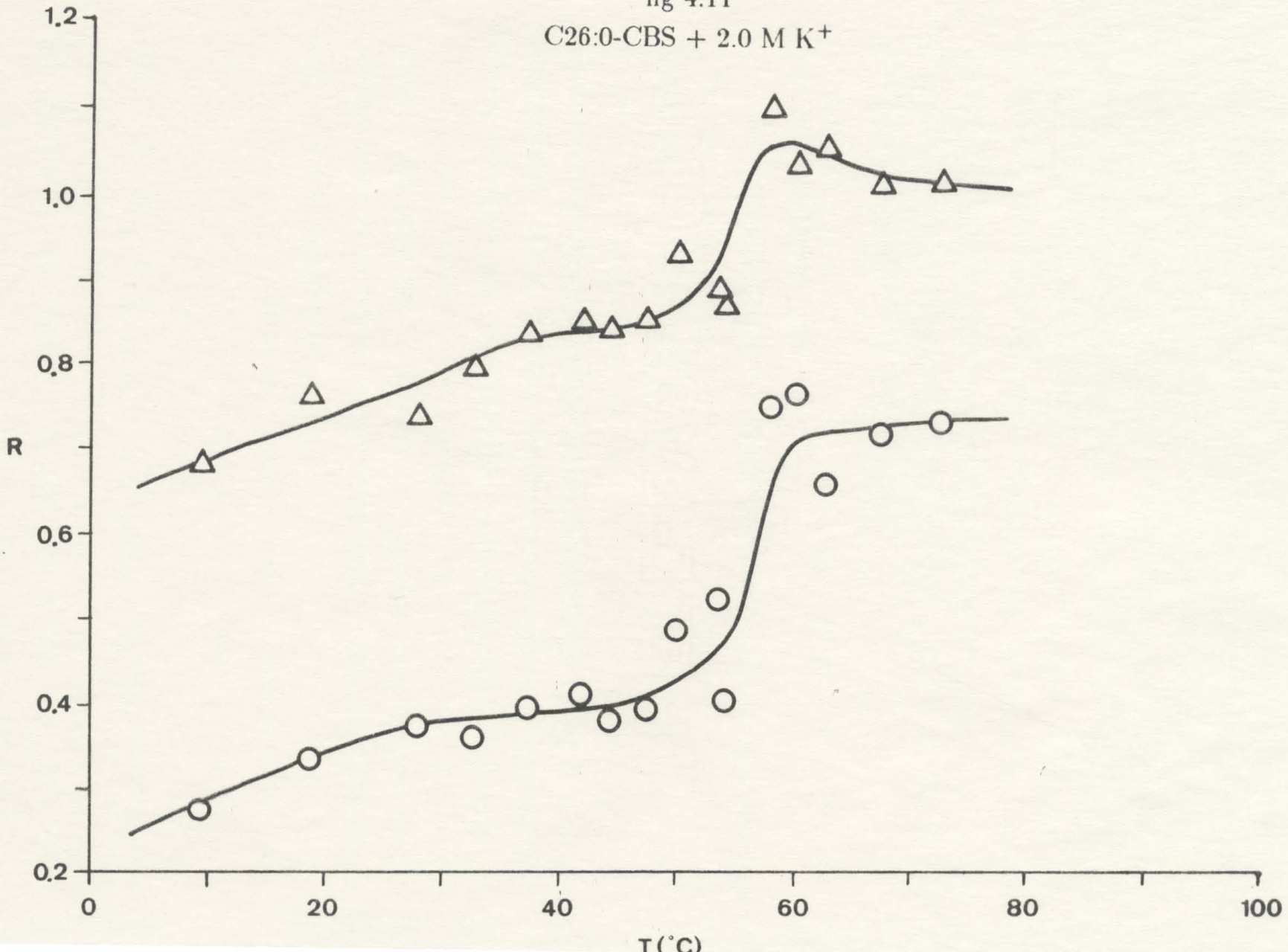

The DSC results of Boggs and her group differ considerably from these reported values. They found that upon heating a single large enthalpy event occurred at T_m =59.9° C and a large event, and then two small events, occurred at 60.5,56.7,and54.9° C upon cooling back down from the liquid crystalline phase in 2 M Li^+. In In 2 M K^+ they observed three transitions at 68.8, 71.5, and 74.8° C upon heating and two events, at 67 and 63° C, upon cooling [27]. The resulting discrepancies between these results and those for this system obtained here cannot at present be adequately explained. No Raman spectra were collected in which the samples were cooled from the fluid phase, and so hysteresis effects in all of these CBS samples were not investigated.

4.8 C18:0h-CBS in 2 M K^+

While the large, broad background supposedly associated with the O-H stretching at the headgroups is observed for all the dispersions investigated, for Raman spectra of C18:0h-CBS the feature proved to be markedly more intense and situated almost exactly beneath the C-H stretching modes. This made subtraction of the feature very difficult as the greatest change in curvature for the feature couldn't be explicitly fitted against, and as a result the extracted Raman spectra were very noisy. Also observed in most of the CBS spectra collected, above T_m this background contour generally seemed to broaden and lessen in intensity. This made removal of the feature somewhat easier for these spectra, although as seen in fig. 4.12 the resulting temperature profiles for C18:0h-CBS in 2 M K^+ are still mostly indeterminate.

There is an indication in the profiles of a change in the temperature sensitivity at 75–80° C. However, it is entirely possible that this is a reflection of the fact that the character of the background peak changes in this temperature range. If it is safe to interpret the background feature as arising from headgroup hydrogen bonding interactions that change at T_m, then for this system we adopt this temperature as an estimate of the main gel-fluid phase transition temperature. Boggs *et.al.* report that upon heating at 10° C/min. this system undergoes

an enthalpy event at 67.0° C and a larger one at T_m =83.4° C. They interpret this ≈20° C increase in T_m over that for the non-hydroxylated lipid version of this system as indication that indeed the additional OH group increases the hydrogen bonding interactions occurring at the headgroup region, aided by the increased shielding effects of the K^+ cation.

4.9 C18:0- and C18:0h-CBS in 0.5 M Li^+

As seen in fig. 4.13 and 4.14, both the hydroxylated and non-hydroxylated forms of C18:CBS behave very similarly. The visual appearance of both the R_1 and R_2 spectral parameter versus temperature curves are essentially identical, all four indicating T_m =53 or 54° C. The two profiles in the non-hydroxylated lipid system profiles seem shifted to higher order by a value of 0.1 with respect to those in fig. 4.13; as the transition temperatures or profile shapes are not affected by this shift, it seems to have little physical relevance and we can conclude that, according to the observations made here, the equilibrium phase behavior of these two systems is identical and that here the presence of the additional OH group makes little difference. It is possible that, as the Li^+ cation seems to shield the repulsive headgroup sulphate charge to a lesser degree than K^+, this additional OH is prevented from engaging in interheadgroup hydrogen bonding interactions for a similar reason as to why T_m is ≈10° C lower in Li^+ than in K^+.

Again reference is made to the DSC results available for CBS. Here it is found that, even in 2 M Li^+, C18:0-CBS did not form the higher-temperature phase described by Boggs *et.al.* as a stable phase at 83.4° C that was seen in 2 M K^+ upon heating.

4.10 C26:0-CBS in 0.5 M Li^+ and K^+

The relevant profiles, contained in figs. 4.15 and 4.16, follow the behavior noted in most of the other CBS systems studied in the more concentrated 2 M cation dispersions. They show single transitions at 52 and 51° C in the R_1 and R_2

figures 4.12, 4.13

Temperature profiles for C18:0h-CBS, in 2 M K^+ and 0.5 M Li^+ respectively.

fig. 4.12

C18:0h-CBS + 2.0 M K^+

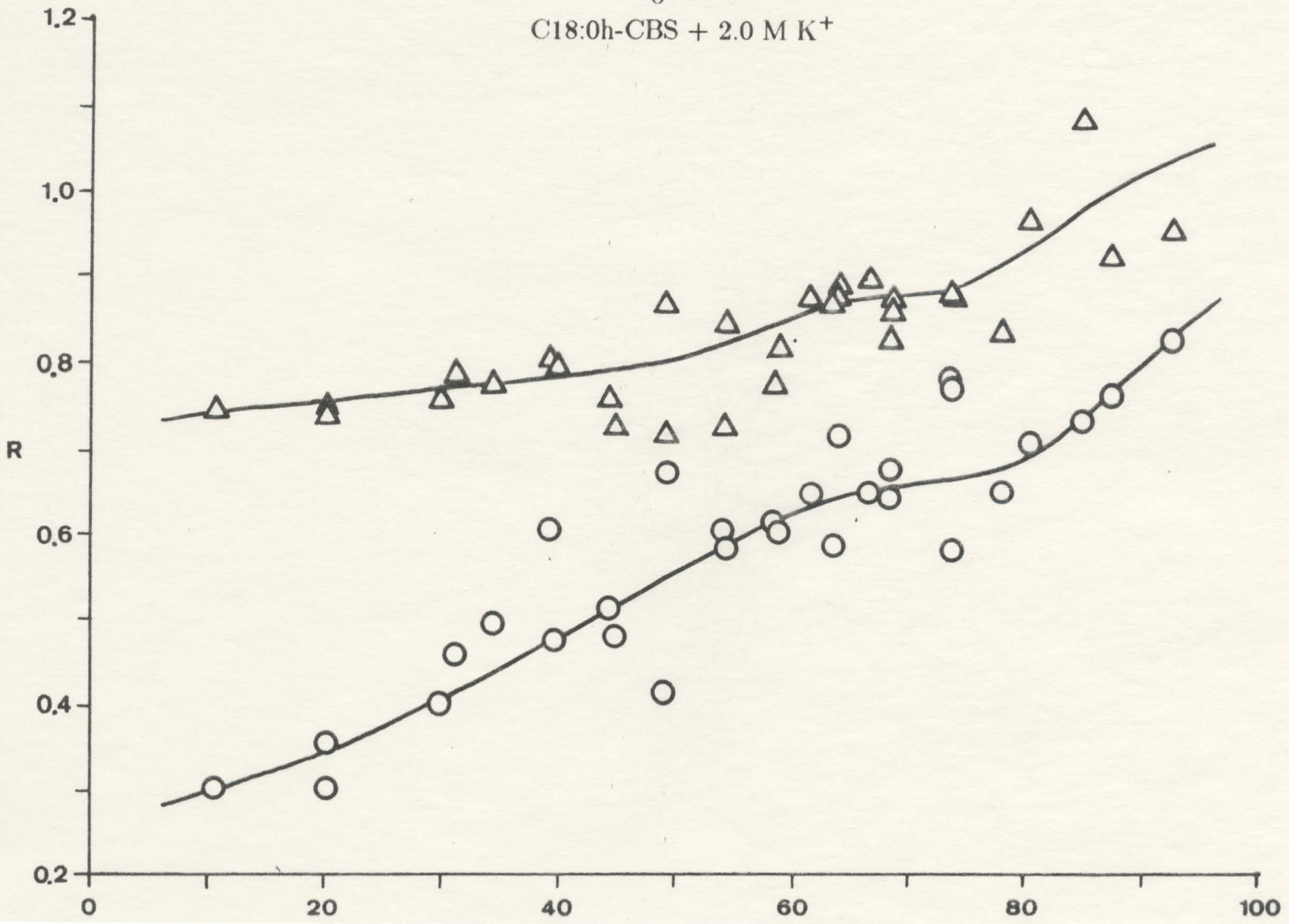

fig. 4.13

C18:0h-CBS + 0.5 M Li^+

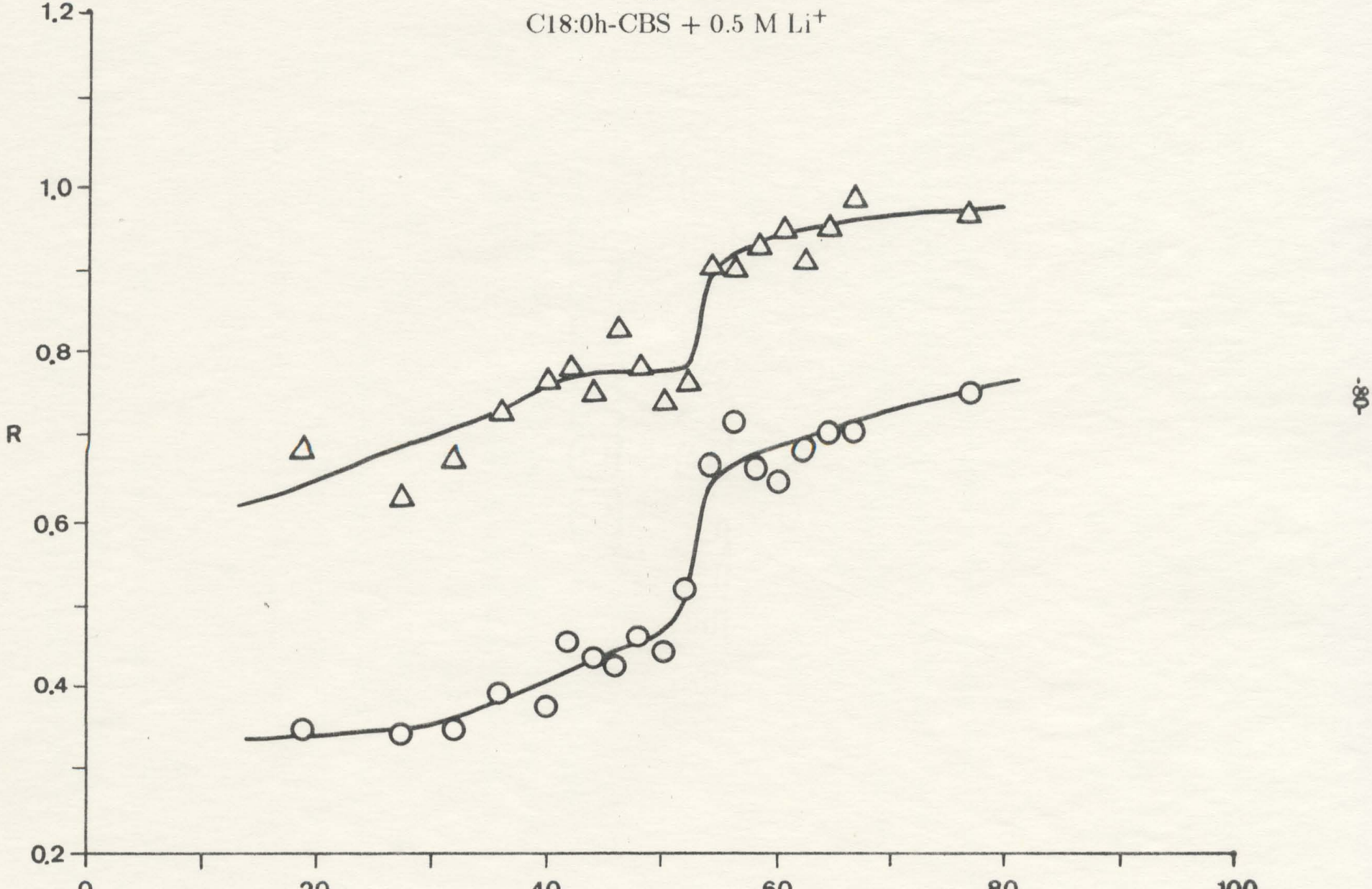

data in Li^+ and 63° C for both curves in 0.5 M K^+. This is somewhat contrary to expectations, as a decrease in cation concentration should produce a decrease in T_m as the repulsive effects between the headgroups are shielded less and less. The result here suggests that perhaps even at 0.5 M concentrations the maximum degree of shielding for either cation has already been reached; this is discussed later.

Earlier it was noted that for these lower concentration samples long term storage effects might be present. Relative to the profiles in the 2 M cation dispersion both R_1 and R_2 in fig. 4.15 and R_1 in fig. 4.16 are very flat and representative of a highly ordered bilayer phase below T_m. It has been suggested that this might be indicative of the formation of a dehydrated lipid phase during storage. Additionally, since the cation effect on T_m persists, the bilayers seem to become fully hydrated prior to the main lipid transition.

4.11 Discussion

Before discussing the results described for the CBS thermal profiles, a discussion of the background feature encountered in the course of this investigation is in order. In an attempt to isolate the cause of the massive background feature underlying the C-H stretching region in all of the CBS Raman spectra collected, a survey of spectra of various systems was undertaken with the assistance of J. Jerrett at Memorial University. Among the systems examined were pure water, the 2.0 M ionic solutions used to disperse the CBS lipids, a 3 M solution of sucrose in water, pure ethanol, and a dispersion in water of variable-chainlength phosphatidyl inositol extracted from natural sources. Also examined were D_2O, and a dispersion of C18:0-CBS in D_2O.

The Raman spectrum of pure H_2O at 11° C showed the O-H stretching feature lying between 3000 cm^{-1} and 3700 cm^{-1} with a shoulder at 3225 cm^{-1} and a maximum at 3450 cm^{-1}, some 400 cm^{-1} beyond the observed maximum in the CBS spectra on average. Upon freezing, the shoulder and peak in this

figures 4.14-4.16

Temperature profiles, as in figs. 4.4-4.11, for non-hydroxylated CBS in 0.5 M cation solutions.

fig. 4.14
C18:0-CBS + 0.5 M Li^+

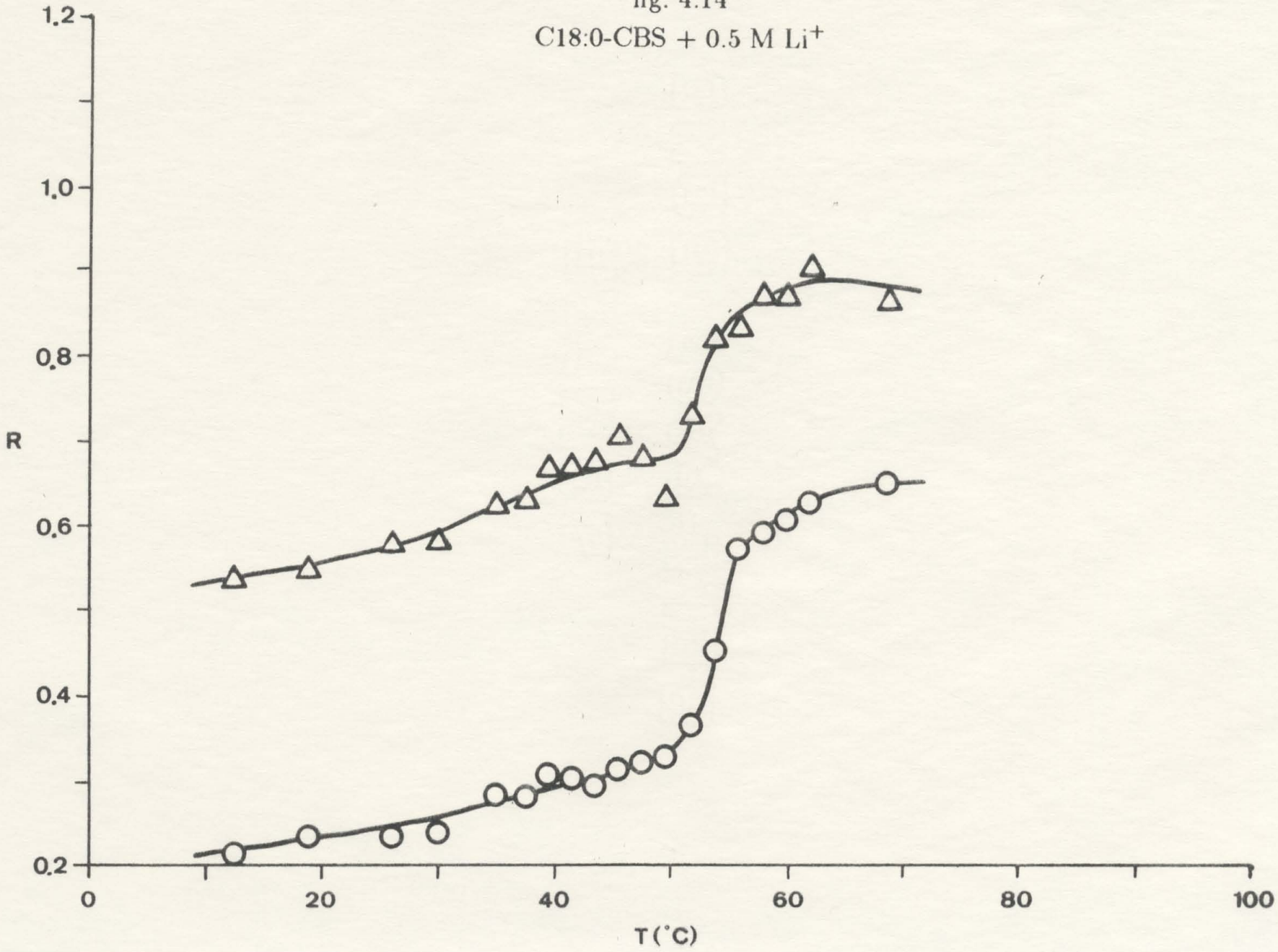

fig. 4.15
C26:0-CBS + 0.5 M Li^+

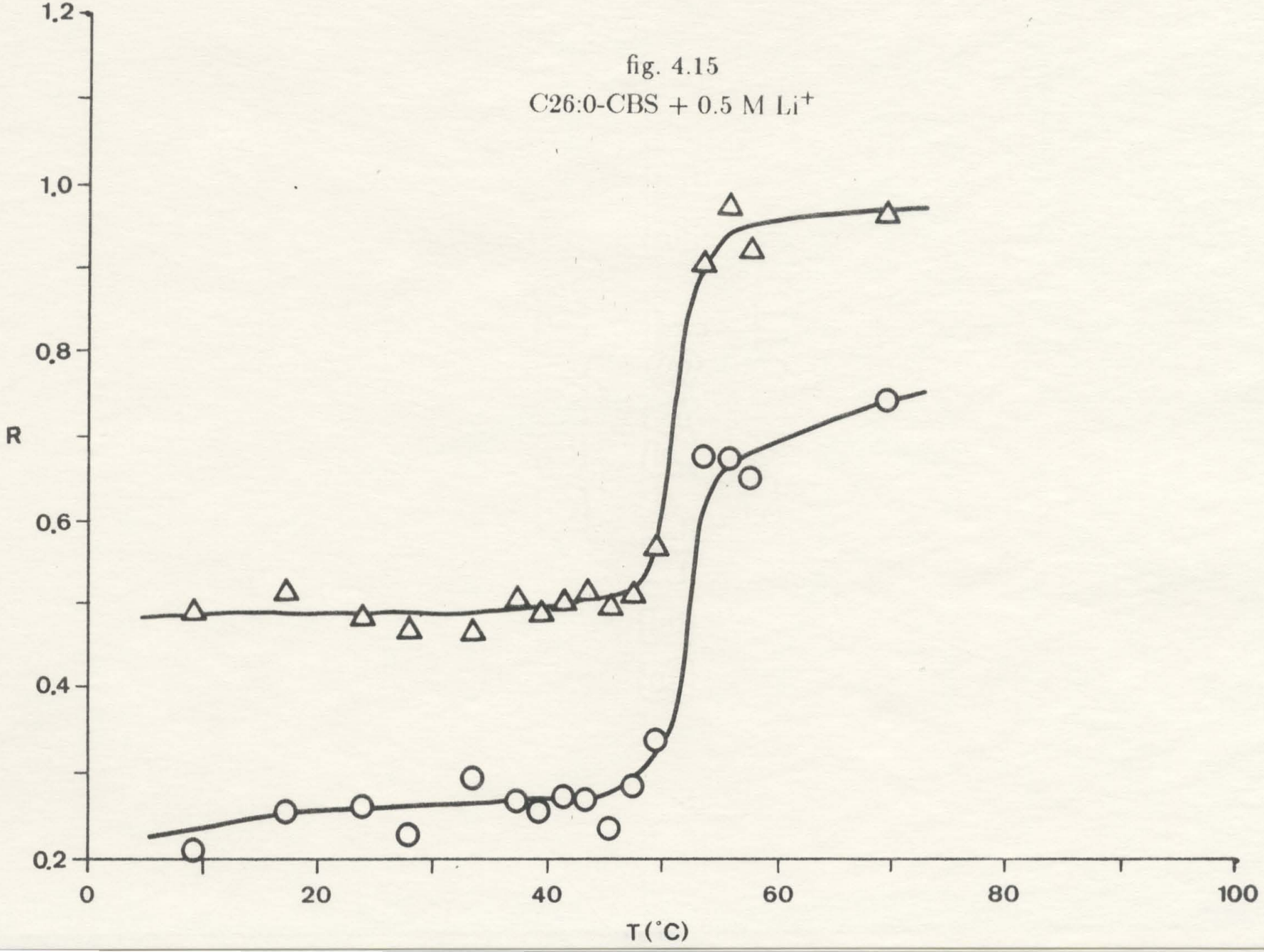

fig. 4.16

C26:0-CBS + 0.5 M K^+

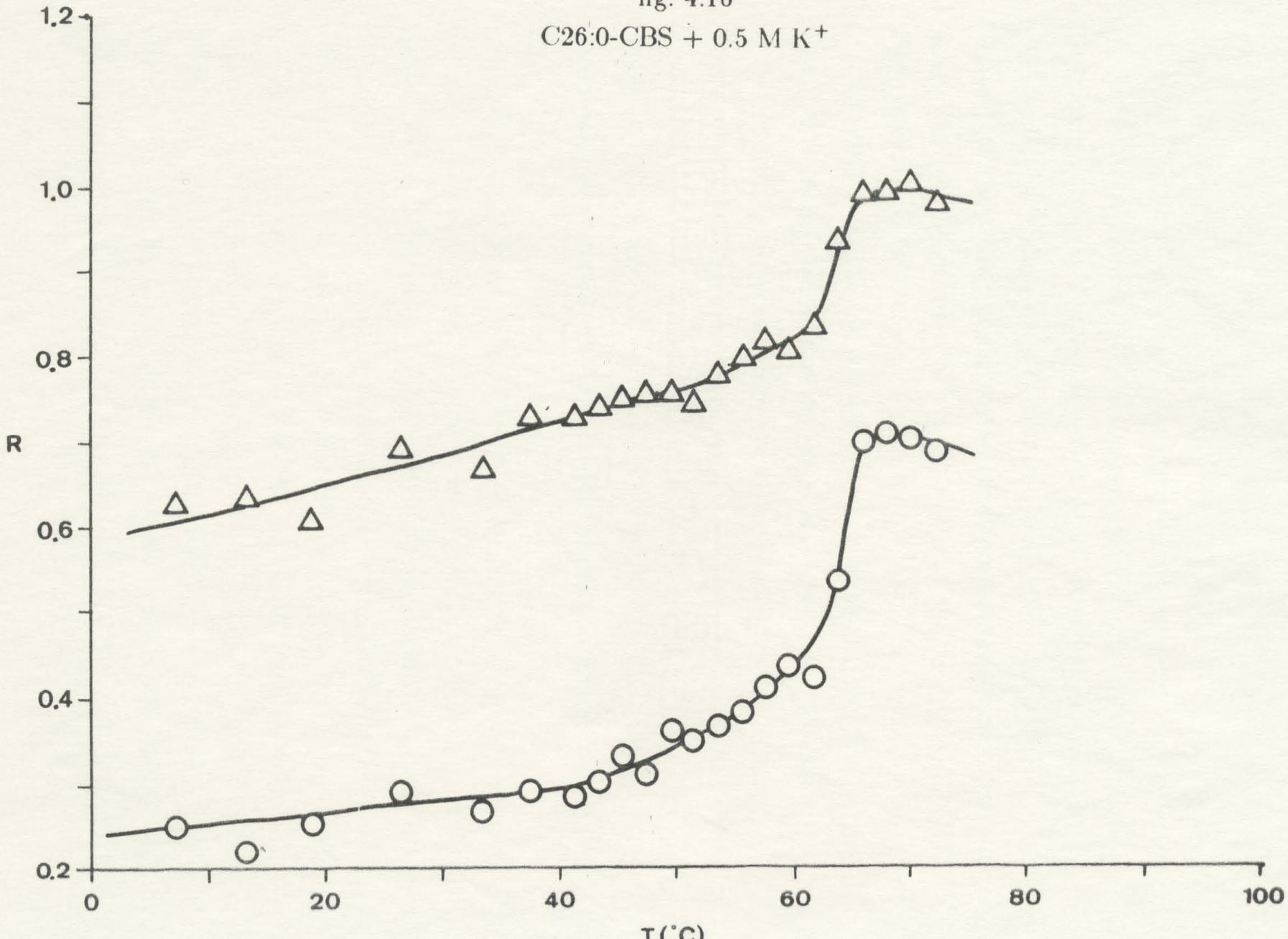

stretching feature became more sharply defined and reversed positions, occurring at 3350 cm^{-1} and 3140 cm^{-1} respectively, which is still beyond the CBS background peak. This behavior has been documented in the literature (for example, see [41]) by other researchers. The presence of 2.0 M K^+ or Li^+ seemed not to affect either the location of this feature or its contour to any appreciable amount, at least at temperatures between 10 and 60° C. Raman spectra of sucrose in H_2O showed three C-H stretching features at 2900, 2940, and 2970 cm^{-1}, well separated from the O-H stretching feature. Ethanol spectra did not show any appreciable evidence of O-H stretching at all, but the molecule's C-H stretching region was well resolved.

The Raman spectra of the phosphatidyl inositol (PI) dispersion, which involves a headgroup based on a sugar residue linked through a phosphate group to the glycerol and acyl chains, were similar to the sucrose spectra in that the O-H band was not at all intense and was removed from the C-H stretching region. Phosphatidyl choline (PC) dispersion spectra also show the water band clearly, though as was the case with the PI and sugar spectra this band was much less intense than the C-H region as a whole and adjacent to it, not superposed with it.

D_2O spectra look much like water spectra, except that the D-O stretching band was located between 2200 and 2700 cm^{-1}, as expected. When a sample of C18:0h-CBS was prepared in D_2O and run in the spectrometer, however, there was still present at $\approx$2900 cm^{-1} a very intense background feature, very much like the O-H band for water in appearance. The D_2O band was also evident. This in itself seems to indicate that most if not all of this background band arises from the lipid molecules, which contain OH groups, as opposed to a D-O stretch between the lipid headgroups and the D_2O. Caution must be exercised in this interpretation because deuteron-proton exchange can take place between the lipid and its aqueous environment fairly quickly with the result that significant amounts of H_2O can appear in the buffer. Nevertheless, the magnitude of the

feature in both D_2O and H_2O is very similar at comparable temperatures. The fact that this feature is most intense for dispersions of hydroxylated CBS is also in agreement with this interaction argument, as is the observation that the shift in frequency of the feature is greatest for hydroxylated CBS.

A final observation is the fact that, without exception, this background feature is drastically modified upon the transition of the CBS bilayers into their liquid crystalline states. The broad feature is centered at $\approx$3000 cm^{-1} for the non-hydroxylated CBS dispersions and $\approx$2900 cm^{-1} for C18:0h-CBS in 2 M K^+ only, with a shoulder at $\approx$3400 cm^{-1}. At T_m the intensity of this peak falls off markedly, and the feature broadens even further; the component forming the shoulder seems little-changed, and it becomes clear that this is just the O-H stretching mode of the excess H_2O in the lipid dispersion re-emerging from the rest of the background (see fig. 4.17). An explanation for this behavior might be as follows; in the fluid phase the headgroups of lipid molecules interact less strongly with one another due in part to increased repulsive effects between the hydrocarbon chains as *gauche* conformers arise in them, so that the two-dimensional lateral motion associated with lipids in this phase occurs. Any hydrogen bonding effects between adjacent headgroups would be lessened both by physical separation and screening effects of the cations in the buffer. If this background feature arises due to such interactions, it would be expected to decrease in magnitude upon the system entering the liquid crystalline phase.

In all of the non-hydroxylated CBS - cation systems studied at thermal equilibrium, the main gel-LC transition temperature T_m was always $\approx$50–55° C in the presence of 2.0 M Li^+ and $\approx$60–65° C for a similar concentration of K^+. Thus it would seem that headgroup effects are more important in establishing the main transition temperature than the lengths of the acyl chains, contrary to the case for the non-charged phospholipids such as PC's with either symmetric of asymmetric chain lengths [12,23]. As an example of the magnitude of the effect of chain length in PC's, dimyristoyl PC (14 carbon chains) has a transition temperature of 23.8° C, dipalmitoyl PC (16 carbon chains) has $T_m = 41.1°$ C as

figure 4.17

Changes in the raw Raman spectral profiles for C18:0-CBS in 2 M Li^+ at three temperatures. Note the abrupt drop in magnitude of the large O-H stretch - like background feature when the lipid bilayer transitions into the fluid phase.

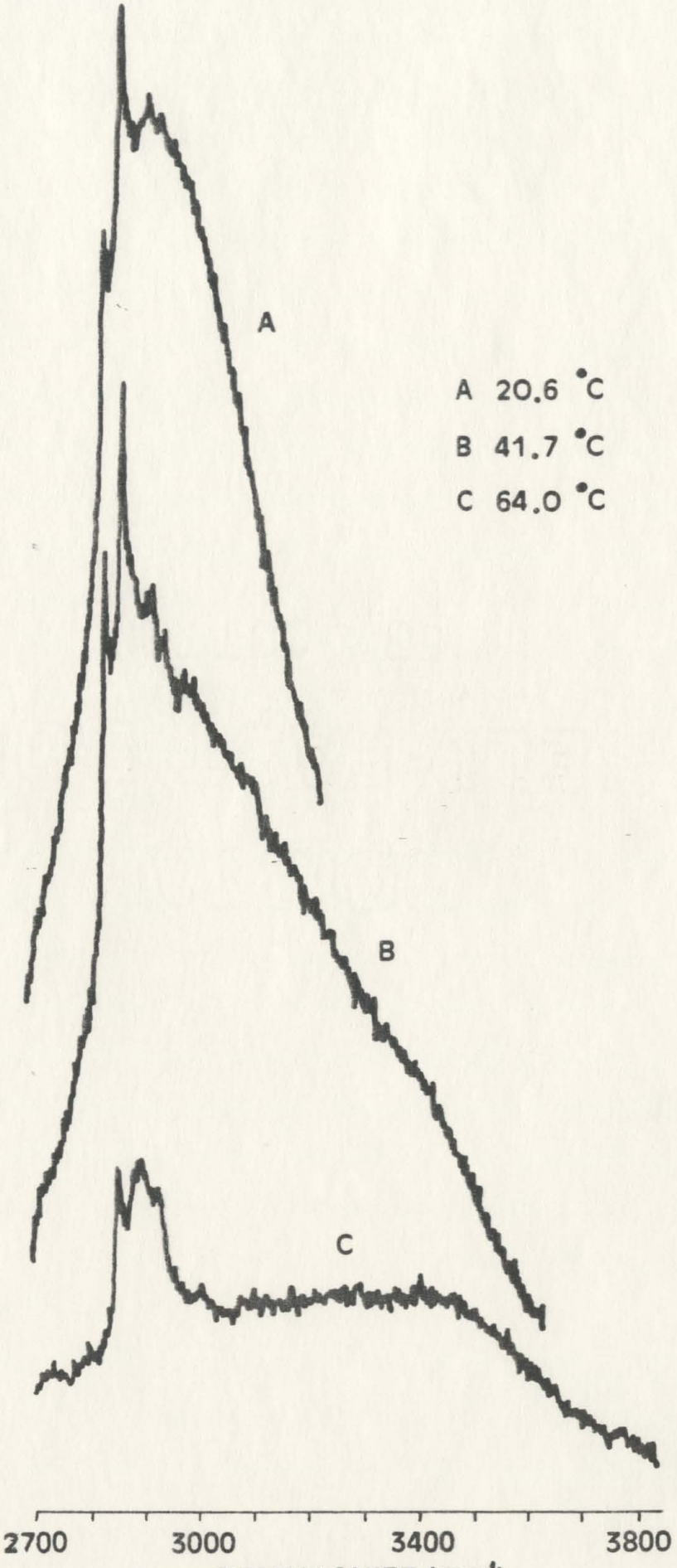
A
B
C
A 20.6 °C
B 41.7 °C
C 64.0 °C
2700
3000
3400
3800

mentioned earlier, and distearoyl PC (18 carbon chains) has $T_m = 53.5^o$ C. The increase in T_m for the various non-hydroxylated species of CBS studied follows a decrease in the hydrated ionic radius of K^+ over that of Li^+. K^+ tends to have a greater affinity for the negatively-charged sulphate in CBS than Li^+, and consequently shields this charge to a larger extent with the result that inter-headgroup repulsion becomes lesser and the integrity of the bilayer increases.

In light of the above, it would be expected that the concentration of the cation used in preparing the dispersions also has an affect on T_m. This effect is not observed in the present data, as for example for C18:0-CBS in 0.5 M Li^+ $T_m \approx 53^o$ C (as averaged between the values for the R_1 and R_2 profiles) and in 2 M Li^+ $T_m \approx 49^o$ C. The difference in the main transition temperature here is in the opposite sense to what is expected. Since the 0.5 M dispersion shows increased overall chain ordering as reflected (i) by the disproportionately large $I_{2885\ cm^{-1}}$ values giving rise to the abnormally low values for R_1 and R_2, and (ii) a moderate *increase* in T_m over that in the 2 M dispersion, storage of this sample at 20^o C seems to have a small but definite ordering effect on the bilayers. Turning to the C26:0-CBS results, the measure T_m for this lipid in 2 and 0.5 M Li^+ is ≈ 51 and $\approx 53^o$ C, respectively, and are nearly identical despite the change in the cation concentration. For this CBS species in K^+ there is a difference in the transition temperature, again an increase, from $T_m \approx 56^o$ C in 2 M K^+ to $T_m \approx 63^o$ C in 0.5 m K^+, but T_m for the more concentrated cation dispersion seems too low for reasons that are not understood. The behavior for C26:0-CBS in the half molar cation solution is very similar to that for the C18:0-CBS lipids in the two molar solutions, thus preserving the chain length-independent nature of T_m and the dependence on cation type as previously mentioned, but showing no cation concentration effects.

The reason why a decrease in the cation concentration from 2 to 0.5 molar produced no significant change in the main transition temperature for either of the cations used might be connected with the relatively high value of these

concentrations as compared to those found in natural systems where CBS occurs. If we look at a possible mechanism of the cation-sulphate ion association, we realize that at very low concentration there is a competition between the free H_2O's affinity for the negative charge on the SO_3^- and the water molecules associated with the hydrated cations, resulting in an equilibrium concentration of the cation at the bilayer surface which might be comparable to that in the surrounding aqueous phase. At higher concentrations of cation, however, a saturation point is reached where no further cations become "attached" to the bilayer surface; above this point an increase in the bulk cation concentration will not affect the concentration at the headgroups. The magnitude of the screening effect is still dependent on the cation's effective radius, because in order to screen the SO_3^- charge the cations have to be more or less *between* the headgroups of the CBS molecules which is a more difficult condition to fulfill as the ionic radius increases.

In DSC studies of C16, C18, and C24:0-CBS in Na^+ and K^+ Boggs reports that indeed the trend to higher values for T_m with higher cation concentration levels off [26, fig.3]. This effect is much more pronounced for K^+ in her data than for Na^+, and one would extrapolate even greater than for Li^+, which is larger still in the hydrated state. The saturation point seems to occur at about 0.5 molar for both Na^+ and K^+; in retrospect it would be beneficial to further pursue this phenomena with Raman studies of CBS at cation concentrations lower than 0.5 M. Another variable that might be investigated using Raman scattering is the valency of the cation; DSC studies have previously indicated that in the cations Ca^{2+} and Mg^{2+} CBS bilayers behave similarly as when they exist in the presence of Li^+ [26].

4.12 Summary

In point form the conclusions that can be drawn from the preceding results are as follows;

figure 4.18

Illustration of the inversion in the trend of ionic radius upon hydration of the alkali cations (from Finean, Coleman, and Michell, 1984).

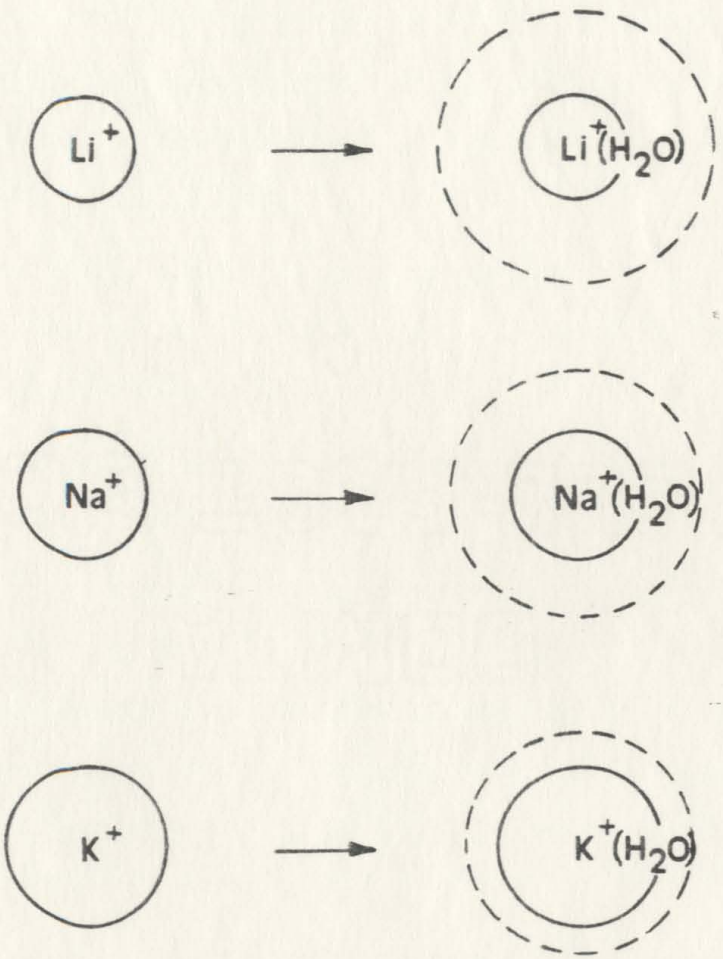
Li+
Li+(H2O)
Na+
Na+(H2O)
K+
K+(H2O)

1. The interactions at the bilayer-water interface between the headgroups and themselves, the headgroups and whatever cation is in the water phase, and the headgroups and the water itself have been shown to be the predominant factors in setting the gross thermotropic behavior of CBS bilayers.

2. $T_m \approx 50–55^\circ$ C for all of the non-hydroxylated CBS dispersions in 2 M Li^+ and $T_m \approx 60–65^\circ$ C for these lipids in 2 M K^+, indicating that the screening effect of these cations on the SO_3^- charge is substantially greater for potassium than for lithium. The degree of screening seems inversely proportional to the hydrated cation radius.

3. That the relative degree of screening between K^+ and Li^+ is apparently unchanged by quartering the concentration of these cations in the CBS dispersion from 2 molar to 0.5 molar seems to indicate that the SO_3^- ions are saturated by bound cations, and screened to nearly the full extent capable by the respective cation.

4. Prolonged storage above the freezing point of the buffers has an increased ordering effect on the bilayers of the 0.5 molar dispersions, which is not removed by heating of the samples to above T_m for 2-5 minutes. Dehydration of the bilayers near T_m is unlikely as the cation screening effects remain through the transition, but it might exist at lower temperatures prior to the main transition.

5. The hydrocarbon chain length asymmetries and their effects upon the interaction between the chains makes possible a variety of packing configurations under different conditions. With the headgroup charge providing some of the repulsive interactions that balance the attractive forces provided through the hydrophobic effect and any hydrogen bonding or Van der Waals forces, not to mention Coulombic interactions, that exist, one might expect there to be lesser constraints on the precise packing scheme adopted by the chains. The presence of K^+ seems to enhance the tendency of CBS bilayers to interdigitate, perhaps by increasing these constraints and making

interdigitated packing more energetically favorable. From ESR studies [28] it has been concluded that the longer-chain CBS species form a stable mixed-interdigitated phase below $\approx$35–45° C, and adopt a metastable partially-interdigitated phase upon cooling from the liquid crystalline phase prior to reaching these temperatures. The observed phase behavior of C24:0-CBS in 2 M K^+ correlates well with that of bilayer systems of the neutral lipid C24:sphingomyelin, showing progressive formation of both of these interdigitated states. The fact that Li^+ seems to inhibit formation of any one stable (interdigitated) phase has been observed by Boggs for this lipid as well [28].

6. The myriad of so-called metastable phases observed by Boggs *et.al.* in their DSC and ESR studies are not seen in the present results; only the formation of the fluid phase from the gel phase is explicitly seen in the thermal profiles in most cases. This probably stems, in short, from the different sample histories for the Raman results, each being essentially a series of short incubations as opposed to those for the DSC scans. The present experiments were performed with the samples always at constant temperature.

7. Adding an OH group to the acyl chain of C18:0-CBS to form C18:0h-CBS appears to increase T_m substantially as seen here in changes of the broad background feature removed prior to analysis of all the CBS spectra, presumably related to headgroup hydrogen bonding interactions, when the lipid is dispersed in K^+ but not in Li^+. Again, the lessening of inter-headgroup Coulombic repulsion through the screening effects of K^+ seems to enable the increased hydrogen bonding associated with this additional hydroxyl group, as opposed to the case for Li^+.

REFERENCES

[1] Gorter,E. and Grendel,F.(1925). *J. exp. Med.* **41,** 439.

[2] Rouser,E., Nelson,G.J., Fleischer,S., and Simon,G.(1968) *in* "Biological Membranes: Physical Fact and Function" (D.Chapman, ed.) pp 5-69. Academic Press Inc.

[3] Singer,S.J.(1975) *in* "Cell Membranes: Biochemistry, Cell Biology and Pathology" (G.Weissmann and R.Claiborne, eds.) pp 35-44. HP Publishing Co., Inc. New York, N.J.

[4] Finean,J.B., Coleman,R., and Michell,R.H.(1984) *in* "Membranes and their Cellular Functions". Blackwell Scientific Publications, Oxford.

[5] Unwin,N., and Henderson,R.(1984) *Sci. Amer.* vol. **250** no. **2.** pp 78-94.

[6] Singer,S.J., and Nicolson,G.L.(1972) *Science* **175,** 720-731.

[7] Houslay,M.D., and Stanley,K.K.(1982) *in* "Dynamics of Biological Membranes". John Wiley & Sons Ltd.

[8] Silvius,J.R., Lyons,M., Yeagle,P.L., and O'Leary,T.J.(1985) *Biochemistry* **24,** 5388-5395.

[9] Chapman,D.(1975) *in* "Cell Membranes: Biochemistry, Cell Biology, and Pathology" (G.Weissmann and R.Claiborne, eds.) pp 13-22. HP Publishing Co. Inc. New York, N.J.

[10] Norton,W.T.(1977) *in* "Myelin" (P.Morrell, ed.) pp 161. Plenum Press, New York.

[11] Dekker,C.J., Geurts van Kessel,W.S.M., Klomp,J.P.G., Pieters,J., and de Kruijff,B.(1983). *Chem. Phys. Lipids* **33,** 93-106.

[12] Levin,I.W.(1984) *in* "Advances in Infrared and Raman Spectroscopy Volume II" (R.J.H. Clark and R.E. Hester, eds.) pp 1-48. Wiley Heyden.

[13] Pink,D.A., Green,T.J., and Chapman,D.(1980) *Biochemistry* **2,** 349.

[14] Lee,A.G.(1977) *Biochim. Biophys. Acta* **514,** 54-68.

[15] Jan,N., Lookman,T., and Pink,D.A.(1984) *Biochemistry* **23,** 3227-3231.

[16] Nagle,J.F.(1980) *Ann. Rev. Phys. Chem.* **31,** 157-195.

[17] Cevc,G., and Marsh,D.(1987) *in* "Phospholipid Bilayers: Physical Principles and Models" pp 21. John Wiley & Sons, Inc.

[18] Janiak,M.J., Small,D.M., and Shipley,G.G.(1979) *J. Biol. Chem.* **254,** 6068-6078.

[19] Silvius,J.R., Brown,P.M., and O'Leary,T.J.(1986) *Biochemistry* **25,** 4249-4258.

[20] Hui,S.W., Mason,J.T., and Huang,C.(1984) *Biochemistry* **23,** 5570-5577.

[21] Ranck,J.L., Keira,T., and Luzzati,V.(1977) *Biochim. Biophys. Acta* **488,** 432-441.

[22] McDaniel,R.V., McIntosh,T.J., and Simon,S.A.(1983) *Biochim. Biophys. Acta* **731,** 97-108.

[23] Huang,C., Mason,J.T., and Levin,I.W.(1983) *Biochemistry* **22,** 2775-2780.

[24] Levin,I.W., Thompson,T.E., Barenholz,Y., and Huang,C.(1985) *Biochemistry* **24,** 6282-6286.

[25] Ki,P.F., and Kishimoto,Y.(1984) *J. Neurochem.* **42,** 994-1000.

[26] Boggs,J.M., Koshy,K.M., and Rangaraj,G.(1984) *Chem. Phys. Lipids* **36,** 65-89.

[27] Boggs,J.M., Koshy,K.M., and Rangaraj,G.(1988) *Biochim. Biophys. Acta* **938,** 361-372.

[28] Boggs,J.M., Koshy,K.M., and Rangaraj,G.(1988) *Biochim. Biophys. Acta* **938,** 373-385.

[29] Mendelsohn,R.(1986) *in* "Spectroscopy in the Biomedical Sciences" (R.M. Gendreau, ed.) pp 151-173. CRC Press.

[30] Lord,R.C., and Mendelsohn,R.(1981) *in* "Membrane Spectroscopy" (E. Grell, ed.) pp 389-412. Springer-Verlag, Berlin, Heidelberg, New York.

[31] Woodward,L.A.(1972) *in* "Introduction to the Theory of Molecular Vibrations and Vibrational Spectroscopy" pp 253-271. Oxford University Press.

[32] Lippert,J.L., and Peticolas,W.L.(1972) *Biochim. Biophys. Acta* **282,** 8-17.

[33] Karvaly,B., and Loshchilova,E.(1977) *Biochim. Biophys. Acta* **470,** 492-496.

[34] Cirak,J., and Horvath,L.I.(1985) *Chem. Phys. Lipids* **36,** 243-252.

[35] Craig,N.C., Bryant,G.J., and Levin,I.W.(1987) *Biochemistry* **26,** 2449-2458.

[36] Snyder,R.G., and Schachtschneider,J.H.(1962) *Spectrochim. Acta* **19,** 85-116.

[37] Schachtschneider,J.H., and Snyder,R.G.(1962) *Spectrochim. Acta* **19,** 117-168.

[38] Schaufele,R.F., and Shimanouchi,T.(1967) *J. Chem. Phys.* **46,** 755.

[39] Tasumi,M., and Shimanouchi,T.(1962) *J. Mol. Spectroscopy* **9,** 261-287.

[40] D'Arrigo,G., Maisano,G., Mallamace,F., Migliardo,P., and Wanderlingh,F.(1981) *J. Chem. Phys.* **75,** 4264-4270.

[41] Walrafen,G.E., Hokmabodi,M.S., and Yang,W.-H.(1986) *J. Chem. Phys.* **85,** 6964-6969.

APPENDIX 1.

```
1   REM ************************************************************************
2   REM *                              FIT6.BAS                                  *
3   REM ************************************************************************
5   REM
10  REM THIS PROGRAM ATTEMPTS TO FIT A 4th-DEGREE POLYNOMIAL APPROXIMATION TO A
15  REM BACKGROUND PROFILE AS SAMPLED FROM 2700 TO 2825cm-1 AND 3000cm-1 TO THE
20  REM END OF FILE IN THE CH2-STRETCHING MODE REGION OF A HYDROCARBON CHAIN
25  REM RAMAN SPECTRUM. THE PROGRAM CALCULATES THE SAMPLE TEMPERATURE USING THE
30  REM THERMISTOR EQUATION AND THE MEASURED THERMISTOR RESISTANCE, SMOOTHES
35  REM THE SPECTRUM CONTOUR, AND DETERMINES THE RAMAN PEAK HEIGHT RATIOS
40  REM ~I2935/I2885 AND ~I2850/I2885. THE RATIO OF THE MAXIMUM OF THE NON-
45  REM CONSTANT PORTION OF THE FITTED BACKGROUND PROFILE AND THE CONSTANT
50  REM ~2850 FEATURE IS CALCULATED; THE BACKGROUND IS THOUGHT DUE TO O-H
55  REM INTERACTION AT THE HEADGROUP OF LIPIDS.
100 REM --------------------LOAD DATA-------------------------
110 DIM Y(1000)
120 INPUT"Raman stretching-mode spectra filename";NAME$
130 OPEN NAME$+".DAT" FOR INPUT AS #1\I=0
140 INPUT#1,RATE\INPUT#1,INTRVL\IF RATE*INTRVL=1 THEN 150
145 PRINT"DATA NOT IN ONE cm-1 INCREMENTS" \ GOTO 9999
150 INPUT#1,XSTART\INPUT#1,RTEMP
160 TKEL=1/(0.00317662+LOG(RTEMP)*0.00028206+(LOG(RTEMP))^3*0.00000259)
170 TCEL=TKEL-273.15
180 INPUT#1,Y(I) \ ON ERROR GOTO 200
190 I=I+1 \ GOTO 180
200 IF ERR=50 THEN Y(I)=Y(I-1) \ RESUME 190
210 IF ERR<>11 THEN ON ERROR GOTO 0 ELSE RESUME 220
220 N=I \ PRINT\PRINT"Finished. Loaded";N;"points,"
230 PRINT XSTART;"cm-1 to ";XSTART+N;"cm-1"
240 PRINT"Sample at";TKEL;"K"
245 PRINT"       or";TCEL;"deg. C"
250 GOSUB 1400
260 INPUT"NUMBER OF PASSES";PASS
270 FOR P=1 TO PASS
280 RESTORE
300 REM -------LEAST SQUARES FOURTH DEGREE POLYNOMIAL FIT-------
302 REM (Fit data shifted to origin; approx. of Maclauren series)
303 REM (truncated to n=4. Sampled data near Raman is automatically)
304 REM (weighted against somewhat by sampling gap.)
305 S0=0\S1=0\S2=0\S3=0\S4=0\S5=0\S6=0\S7=0\S8=0
306 T0=0\T1=0\T2=0\T3=0\T4=0
307 FOR J=0 TO 1
308 READ XL\IF J=0 THEN XL=XSTART+5
310 READ XR\IF J=1 THEN XR=XSTART+N-5\PRINT XL;XR;
312 IF J=1 AND XSTART+N<3040 THEN XL=3010
315 FOR XX=XL TO XR\X=(XX-3000)/1000
320 S0=S0+1    \ S1=S1+X    \ S2=S2+X^2
322 S3=S3+X^3 \ S4=S4+X^4 \ S5=S5+X^5
324 S6=S6+X^6 \ S7=S7+X^7 \ S8=S8+X^8 \I=XX-XSTART
326 T0=T0+Y(I)     \ T1=T1+X*Y(I)
328 T2=T2+X^2*Y(I) \ T3=T3+X^3*Y(I) \ T4=T4+X^4*Y(I)
330 NEXT XX \ NEXT J\PRINT S0;"Points sampled"
332 Q1=S1*S1-S2*S0 \ Q2=S1*S2-S3*S0 \ Q3=S1*S3-S4*S0
```

```
334 Q4=S1*S4-S5*S0 \ Q5=S2*S2-S4*S0 \ Q6=S2*S3-S5*S0
336 Q7=S2*S4-S6*S0 \ Q8=S3*S3-S6*S0 \ Q9=S3*S4-S7*S0
338 Q10=S4*S4-S8*S0 \ R1=S1*T0-T1*S0 \ R2=S2*T0-T2*S0
340 R3=S3*T0-T3*S0 \ R4=S4*T0-T4*S0
342 U1=Q2*Q2-Q1*Q5 \ U2=Q2*Q3-Q1*Q6 \ U3=Q2*Q4-Q1*Q7
344 U4=Q3*Q3-Q1*Q8 \ U5=Q3*Q4-Q1*Q9 \ U6=Q4*Q4-Q1*Q10
346 V1=Q2*R1-R2*Q1 \ V2=Q3*R1-R3*Q1 \ V3=Q4*R1-R4*Q1
348 B1=U2*U2-U1*U4 \ B2=U2*U3-U1*U5 \ B3=U3*U3-U1*U6
350 C1=U2*V1-U1*V2 \ C2=U3*V1-U1*V3
355 A4=(B2*C1-C2*B1)/(B2*B2-B3*B1)
360 A3=(C1-B2*A4)/B1
365 A2=(V1-U3*A4-U2*A3)/U1
370 A1=(R1-Q4*A4-Q3*A3-Q2*A2)/Q1
375 A0=(T0-S4*A4-S3*A3-S2*A2-S1*A1)/S0
500 REM --------------SUBTRACT BACKGROUND-----------------
510 FOR XX=XSTART TO XSTART+N\X=(XX-3000)/1000
520 YBCK=A0+A1*X+A2*X^2+A3*X^3+A4*X^4
530 I=XX-XSTART \ Y(I)=Y(I)-YBCK \ NEXT XX
535 YMIN=0
540 FOR X=2755 TO 2799 \ XT=X-XSTART
545 YMIN=YMIN+Y(XT)/45 \ NEXT X
550 PRINT"YMIN=";YMIN
560 PRINT"FINISHED PASS ";P \ NEXT P
710 XLO=XSTART
720 INPUT"Cut display window to 3100 cm-1";Q$
725 IF Q$="N" OR Q$= "n" THEN XHI=XSTART+N ELSE XHI=3100
730 XLNGTH=XHI-XLO\GOSUB 1000
800 REM --------------FIND 1ST THREE PEAKS-----------------
805 P1Y=0\P2Y=0\P3Y=0
810 FOR X=2830 TO 2860\XR=X-XSTART
820 IF Y(XR)>P1Y THEN P1Y=Y(XR)\P1X=X\END IF\NEXT X
823 X=(P1X-3000)/1000\XX=P1X-XSTART\P1Y=P1Y-YMIN
825 P1YERR=SQR((Y(XX)+A0+A1*X+A2*X^2+A3*X^3+A4*X^4+A5*X^5)/NP)
830 FOR X=2860 TO 2900\XR=X-XSTART
840 IF Y(XR)>P2Y THEN P2Y=Y(XR)\P2X=X\END IF\NEXT X
843 X=(P2X-3000)/1000\XX=P2X-XSTART\P2Y=P2Y-YMIN
845 P2YERR=SQR((Y(XX)+A0+A1*X+A2*X^2+A3*X^3+A4*X^4+A5*X^5)/NP)
850 FOR X=2925 TO 2945\XR=X-XSTART
860 IF Y(XR)>P3Y THEN P3Y=Y(XR)\P3X=X\END IF\NEXT X
863 X=(P3X-3000)/1000\XX=P3X-XSTART\P3Y=P3Y-YMIN
865 P3YERR=SQR((Y(XX)+A0+A1*X+A2*X^2+A3*X^3+A4*X^4+A5*X^5)/NP)
870 PRINT;\CALL MOVABS(0%,730%)\CALL ANMODE
872 RA1=P1Y/P2Y
874 RA1ERR=SQR((P1YERR/P1Y)^2+(P2YERR/P2Y)^2)*RA1
876 PRINT"I";P1X;"/I";P2X;"=";RA1;"+/-";RA1ERR
880 PRINT;\CALL MOVABS(0%,700%)\CALL ANMODE
882 RA2=P3Y/P2Y
884 RA2ERR=SQR((P3YERR/P3Y)^2+(P2YERR/P2Y)^2)*RA2
885 PRINT"I";P3X;"/I";P2X;"=";RA2;"+/-";RA2ERR
890 GOSUB 1700\PRINT;\CALL MOVABS(0%,670%)\CALL ANMODE
895 PRINT"IBCK/I";P1X;"=";YBM/P1Y
999 SLEEP 60\GOTO 9999
1000 REM ----------------DISPLAY SUBROUTINE--------------------
1005 FOR X=2830 TO 2860\XR=X-XSTART
```

```
1010 IF Y(XR)>P1Y THEN P1Y=Y(XR)\P1X=X\END IF\NEXT X
1030 CALL INITT(240%)\BOT=YMIN-P1Y*.1
1040 CALL DWINDO(XLO,XHI,BOT,P1Y*1.8)\CALL TWINDO(0%,1023%,50%,780%)
1050 CALL MOVEA(XLO,Y(XLO-XSTART))
1060 FOR X=XLO TO XHI\CALL DRAWA(X,Y(X-XSTART))\NEXT X
1070 DX=INT(XLNGTH/100)*10\IF DX<20 THEN DX=20
1080 PRINT\CALL MOVEA(XLO,BOT)\CALL DRAWA(XHI,BOT)
1090 FOR X=XLO+DX TO XHI-DX STEP DX
1100 XS%=INT(1023*(X-XLO)/XLNGTH)
1110 CALL MOVABS(XS%,50%)\CALL DRWABS(XS%,35%)\PRINT;
1120 CALL MOVABS(XS%-35%,20%)\CALL ANMODE\PRINT INT(X);
1130 NEXT X
1140 CALL MOVABS(400%,0%)\CALL ANMODE\PRINT"RAMAN SHIFT (cm-1)";
1150 CALL MOVABS(0%,770%)\CALL ANMODE\PRINT NAME$;
1155 PRINT" at";TCEL;"deg. C";
1160 RETURN
1400 REM ---------SAMPLE DATA FOR STANDARD DEVIATION----------
1405 YAVG=0\C1=0
1410 FOR X=2750 TO 2769 \ XT=X-XSTART
1420 YAVG=YAVG+Y(XT)/20 \ NEXT X
1425 PRINT"Mean background(2750-2770)=";YAVG;" counts"
1430 FOR X=2750 TO 2769 \ XT=X-XSTART
1440 C1=C1+(YAVG-Y(XT))^2 \ NEXT X
1450 SIG1=SQR(C1/20) \ SIG2=SQR(YAVG)
1460 PRINT"Background standard deviations:"
1465 PRINT"  sigma(sampled)=";SIG1;" or ";100*SIG1/YAVG;"%"
1467 PRINT"  sigma(Poisson)=";SIG2;" or ";100*SIG2/YAVG;"%"
1468 PRINT"  ratio=";SIG1/SIG2
1500 REM ---------------SMOOTH SUBROUTINE----------------------
1510 INPUT"SMOOTH DATA OVER 1,3,5, OR 7 POINTS";NP\DN=INT(NP/2)
1520 DIM YTMP(N)
1530 FOR X=XSTART+DN TO XSTART+N-DN
1540 XT=X-DN-XSTART\XR=X-XSTART
1550 FOR I=-DN TO DN
1560 YTMP(XT)=YTMP(XT)+Y(XR+I)/NP
1570 NEXT I
1580 NEXT X
1590 FOR X=XSTART+DN TO XSTART+N-DN\XT=X-DN-XSTART\XR=X-XSTART
1600 Y(XR)=YTMP(XT)
1610 NEXT X
1620 RETURN
1700 REM -------------GET BACKGROUND MAXIMUM-----------------
1710 YBM=0
1720 FOR XX=XSTART TO XSTART+N
1730 X=(XX-3000)/1000
1740 Y=A0+A1*X+A2*X^2+A3*X^3+A4*X^4
1750 IF Y>YBM THEN YBM=Y \END IF\ NEXT XX
1760 RETURN
2000 DATA 2700,2825,3025,3100
9999 END
```

APPENDIX 2.

```
10 REM ************************    TC2    ************************************
20 REM PLOTS TWO ORDER PARAMETERS, R1 AND R2,  ON SAME SET OF AXES.
30 REM **** LOAD DATA FILE ****
40 INPUT"DATA FILE NAME?";N$
50 OPEN N$+".TC2" FOR INPUT AS #1
60 DIM T(100),R(2,100),E(2,100)
70 INPUT#1,T(I),R(1,I),E(1,I),R(2,I),E(2,I)
80 ON ERROR GOTO 100
90 I=I+1\GOTO 70
100 IF ERR<>11 THEN ON ERROR GOTO 0 ELSE RESUME 110
110 N=I-1\PRINT"LOAD SUCCESSFUL.";N;"POINTS."
120 INPUT"PLOT TITLE?";TITLE$
130 CALL INITT(240%)
140 CALL MOVABS(50%,750%)
150 CALL DRWABS(50%,50%)
160 CALL DRWABS(1000%,50%)
170 FOR T=0 TO 100 STEP 10
180   X%=T*9.50+50
190   CALL MOVABS(X%,40%)
200   CALL DRWABS(X%,50%)
210 NEXT T
220 FOR R=0.2 TO 1.2 STEP 0.1
230   Y%=(R-0.2)*700+50
240   CALL MOVABS(40%,Y%)
250   CALL DRWABS(50%,Y%)
260 NEXT R
270 FOR I=1 TO 2
280   FOR J=0 TO N
290     RMAX=R(I,J)+E(I,J)\RMIN=R(I,J)-E(I,J)
300     YMAX%=(RMAX-0.2)*700+50\YMIN%=(RMIN-0.2)*700+50
310     Y%=(R(I,J)-0.2)*700+50\X%=T(J)*9.50+50
320     CALL MOVABS(X%-5%,Y%)
330     CALL DRWABS(X%+5%,Y%)
340     CALL MOVABS(X%,YMAX%)
350     CALL DRWABS(X%,YMIN%)
360   NEXT J
370 NEXT I
380 FOR R=0.2 TO 1.2 STEP 0.2
390   Y%=(R-0.2)*700+50
400   CALL MOVABS(0%,Y%)\PRINT;
410   CALL ANMODE\PRINT R
420 NEXT R
430 FOR T=0 TO 100 STEP 20
440   X%=T*9.50+50
450   CALL MOVABS(X%-30%,20%)\PRINT;
460   CALL ANMODE\PRINT T
470 NEXT T
480 CALL MOVABS(450%,0%)\PRINT;
490 CALL ANMODE\PRINT"T(deg. C)"
500 CALL MOVABS(0%,390%)\PRINT;
510 CALL ANMODE\PRINT"R";
520 CALL MOVABS(400%,760%)\PRINT;
530 CALL ANMODE\PRINT TITLE$
540 SLEEP 60
550 CALL FINITT(0%,767%)
```